

ON THE STRUCTURE AND STABILITY OF RAPIDLY ROTATING FLUID BODIES IN
 GENERAL RELATIVITY. I. THE NUMERICAL METHOD FOR COMPUTING
 STRUCTURE AND ITS APPLICATION TO UNIFORMLY
 ROTATING HOMOGENEOUS BODIES*

E. MANNING BUTTERWORTH AND JAMES R. IPSER

University of Chicago

Received 1975 July 24

ABSTRACT

A new numerical method for computing the structure of rapidly rotating fluid bodies in general relativity is presented. The method is a Henyey-type relaxation method of the kind previously used by Stoeckly in Newtonian theory. It permits the construction of accurate models for fluid bodies with various strengths of relativity and various amounts of uniform or differential rotation. The method is used to construct sequences of uniformly rotating homogeneous bodies, the relativistic analogs of the classical Maclaurin spheroids. The results reveal that, in contrast to the Newtonian sequence, most, and probably all, of the relativistic sequences terminate at nonzero ratios of proper polar radius to proper equatorial radius where centrifugal and gravitational accelerations balance at the equator. Other relativistic effects, including those associated with the formation of regions within which observers must rotate relative to infinity, are discussed. The computational results provide a foundation for a speculative discussion of stability and a scenario for the possible evolution of contracting bodies. Emerging from this are suggestions that relativistic effects might channel the contraction of a highly relativistic body toward a nearly spherical, rather than a disklike, configuration, and that black holes might generally not be near the extreme Kerr limit when they initially form. The computational results are also applied to uniformly rotating neutron stars in order to obtain rough estimates of their rotational energies, their moments of inertia, and the percent by which uniform rotation can increase the maximum-mass limit above its nonrotating value. For equations of state yielding a maximum mass $\sim 1.3 M_{\odot}$ in the nonrotating limit, this latter percent increase is estimated to be ~ 15 percent if attention is restricted to completely stable objects and ~ 30 percent if no stability restrictions are imposed.

Subject headings: relativity — rotation — stars: collapsed

I. INTRODUCTION

This is the first of a series of papers devoted to a study of rapidly rotating systems in general relativity with significant mass-to-radius ratios $2GM/c^2R \gtrsim 0.1$ (G = gravitational constant, c = speed of light), and with significant rotational-energy to potential-energy ratios $\gtrsim 0.1$ (and hence with rotational velocities $v \gtrsim 0.1c$). Such systems are intrinsically interesting to many; and they can be found in a variety of theoretical models for objects such as quasars, the active nuclei of certain galaxies, supernovae, and binary X-ray systems.

Kerr's (1963) remarkable analytic discovery, which has turned out to be the generic solution in general relativity for stationary rotating black holes, has been exploited to such an extent that, today, a lot is known about the properties of black holes. Much less is known about rapidly rotating relativistic sources (e.g., stars, stellar systems). No reasonable analytic solutions are presently available for such systems—the post-Newtonian corrections to the analytic Newtonian Maclaurin spheroids can be obtained in an analytic but difficult way (Chandrasekhar 1967)—and there appears to be little hope for obtaining analytic solutions in the near future.

Out of necessity, a few groups of investigators have turned to the development of numerical techniques for constructing rapidly rotating relativistic sources in equilibrium. Bardeen and Wagoner (1971) specialized the field equations to a form appropriate to infinitesimally thin, pressureless disks in uniform rotation. They expanded the field equations in powers of a parameter measuring the strength of relativity, and they numerically solved through the tenth power of that parameter. Wilson (1972, 1973) and Bonazzola and Schneider (1974) developed numerical methods for constructing rotating fluid bodies with various pressure-density relations and various amounts of flattening. The steps taken by these latter two sets of workers, while admirable, are open to a certain amount of criticism. Wilson's method, for example, places rather strong restrictions on the distributions of angular momentum and entropy in his models. More importantly, as we shall discuss in more detail later, Wilson approximates the

* Supported in part by the Louis Block Fund at the University of Chicago and by the National Science Foundation under grant MPS 74-17456 to the University of Chicago.

boundary conditions guaranteeing asymptotic flatness by certain ad hoc Newtonian-like conditions; and this might well lead to significant inaccuracies in highly relativistic models. Bonazzola and Schneider's method contains artificial restrictions that cause it to break down in highly relativistic situations before many interesting rotational effects, such as the formation of regions within which observers must rotate relative to infinity, appear.

In hope of stumbling upon new results which may be of some interest, we have developed a new self-consistent iterative method for numerically constructing rapidly rotating fluid bodies in general relativity. Our method permits the construction of accurate models obeying various equations of state and having various amounts of differential or uniform rotation.

In § II of this paper we write down the fundamental structure equations. In § III we describe our method for constructing solutions. In § IV we apply it to study the structure of uniformly rotating homogeneous bodies. We have already reported some of our results for these bodies in a brief *Letter* (Butterworth and Ipser 1975). In future papers we shall study the structure and stability of other types of models.

Concerning our notation and conventions in this series, the metric of spacetime has signature $-+++$; $G = c = 1$; Greek tensor indices are associated with spatial coordinates and range from 1 to 3, while Latin tensor indices range from 0 to 3; a comma followed by a coordinate symbol, when used as a subscript, denotes a partial derivative.

II. THE FUNDAMENTAL EQUATIONS OF STRUCTURE

a) Basic Assumptions

In this series of papers we shall be interested in perfect-fluid stellar models whose equilibria have the following properties: (i) a given model is a nonsingular solution of the fully nonlinear Einstein field equations; (ii) the model is stationary, so that a Killing field ξ^a fills spacetime and is timelike, if not everywhere, at least at large spatial separations from the source; (iii) the model is axially symmetric, so that another Killing field η^a also fills spacetime, vanishes on a timelike 2-surface (the axis of symmetry), is spacelike everywhere else, and has integral curves that are topologically circles; (iv) the Killing fields commute,

$$\xi^a \nabla_a \eta^b - \eta^a \nabla_a \xi^b = 0, \quad (1)$$

where ∇_a is the natural covariant derivative; (v) the model is generally rotating rapidly and differentially, and the 4-velocity of the fluid is a linear combination of the two Killing vectors (no meridional circulation); (vi) the geometry possesses a discrete symmetry under reflection through an equatorial plane.

It follows that the local 2-flats spanned by the Killing vectors, and also the orthogonal 2-flats, are surface forming (see, e.g., Carter 1973). The line element can then be written as

$$ds^2 = g_{ab} dx^a dx^b = -e^{2\nu} dt^2 + r^2 \sin^2 \theta B^2 e^{-2\nu} (d\varphi - \omega dt)^2 + e^{2\zeta - 2\nu} (dr^2 + r^2 d\theta^2), \quad (2)$$

which is essentially the form chosen by Bardeen and Wagoner (1971). The time coordinate t ($-\infty \leq t \leq +\infty$) and the azimuthal coordinate φ ($0 \leq \varphi \leq 2\pi$) are adapted to the Killing vectors in the sense that $\nabla^a t$ and $\nabla^a \varphi$ lie in the 2-surfaces spanned by the Killing vectors, and

$$\begin{aligned} \xi^a \nabla_a t &= \eta^a \nabla_a \varphi = 1, \\ \xi^a \nabla_a \varphi &= \eta^a \nabla_a t = 0. \end{aligned} \quad (3)$$

The derivatives $\nabla^a r$ and $\nabla^a \theta$ of the radial coordinate r ($0 \leq r \leq \infty$) and of the angular coordinate θ ($0 \leq \theta \leq \pi$) span the 2-surfaces orthogonal to the Killing vectors. The metric functions ν , B , ω , and ζ are functions of r and θ only. Condition (vi) above means that all metric functions are invariant under $\theta \rightarrow \pi - \theta$.

b) The Field Equations and the Equations of Motion

Many workers have written down the Einstein field equations appropriate to rapidly rotating fluids. In particular, Bardeen and Wagoner (1971) projected the field equations onto the tetrad of Bardeen's (1970) zero-angular-momentum observer (the ZAMO, whose 4-velocity λ^a satisfies $\lambda^a \eta_a = 0$), and obtained the following set of equations, which we shall use:

$$D \cdot (BD\nu) = \frac{1}{2} r^2 \sin^2 \theta B^3 e^{-4\nu} D\omega \cdot D\omega + 4\pi B e^{2\zeta - 2\nu} \left[\frac{(\epsilon + p)(1 + v^2)}{1 - v^2} + 2p \right], \quad (4a)$$

$$D \cdot (r^2 \sin^2 \theta B^3 e^{-4\nu} D\omega) = -16\pi r \sin \theta B^2 e^{2\zeta - 4\nu} \frac{(\epsilon + p)v}{1 - v^2}, \quad (4b)$$

$$D \cdot (r \sin \theta DB) = 16\pi r \sin \theta B e^{2\zeta - 2\nu} p, \quad (4c)$$

$$\begin{aligned}
\zeta_{,\mu} = & -\{(1 - \mu^2)(1 + rB^{-1}B_{,r})^2 + [\mu - (1 - \mu^2)B^{-1}B_{,\mu}]^2\}^{-1} \\
& \times \left\{ \frac{1}{2}B^{-1}\{r^2B_{,rr} - [(1 - \mu^2)B_{,\mu}]_{,\mu} - 2\mu B_{,\mu}\} \{-\mu + (1 - \mu^2)B^{-1}B_{,\mu}\} \right. \\
& + rB^{-1}B_{,r}[\frac{1}{2}\mu + \mu rB^{-1}B_{,r} + \frac{1}{2}(1 - \mu^2)B^{-1}B_{,\mu}] \\
& + \frac{3}{2}B^{-1}B_{,\mu}[-\mu^2 + \mu(1 - \mu^2)B^{-1}B_{,\mu}] - (1 - \mu^2)rB^{-1}B_{,\mu r}(1 + rB^{-1}B_{,r}) \\
& - \mu r^2(v_{,r})^2 - 2(1 - \mu^2)r\nu_{,\mu}v_{,r} + \mu(1 - \mu^2)(v_{,\mu})^2 \\
& - 2(1 - \mu^2)r^2B^{-1}B_{,r\nu_{,\mu}v_{,r}} + (1 - \mu^2)B^{-1}B_{,\mu}[r^2(v_{,r})^2 - (1 - \mu^2)(v_{,\mu})^2] \\
& + (1 - \mu^2)B^2e^{-4\nu}\{\frac{1}{4}\mu r^4(\omega_{,r})^2 + \frac{1}{2}(1 - \mu^2)r^3\omega_{,\mu}\omega_{,r} \\
& - \frac{1}{4}\mu(1 - \mu^2)r^2(\omega_{,\mu})^2 + \frac{1}{2}(1 - \mu^2)r^4B^{-1}B_{,r\omega_{,\mu}\omega_{,r}} \\
& \left. - \frac{1}{4}(1 - \mu^2)r^2B^{-1}B_{,\mu}[r^2(\omega_{,r})^2 - (1 - \mu^2)(\omega_{,\mu})^2]\right\}. \tag{4d}
\end{aligned}$$

There is also an equation for $\zeta_{,r}$. But it provides no new information, and we shall not write it down.

In these equations $\mu \equiv \cos \theta$ and D is the 3-dimensional derivative operator in a flat 3-space with spherical coordinates r, θ, φ . The fluid variables ϵ and p are the total mass-energy density and the pressure in a frame that comoves with the fluid. The physical velocity v of the fluid relative to the local ZAMO is given in terms of the angular velocity

$$\Omega \equiv u^\varphi/u^t \tag{5}$$

relative to infinity via the relation

$$v = (\Omega - \omega)r \sin \theta B e^{-2\nu}. \tag{6}$$

The above equations are supplemented by the generalization of the Newtonian equations of motion. The expression

$$T^{ab} = (\epsilon + p)u^a u^b + g^{ab}p \tag{7a}$$

for the stress-energy tensor of a perfect fluid, and the components

$$(u_a u_b + g_{ab})\nabla_c T^{bc} = 0 \tag{7b}$$

of the relativistic equations of motion yield the useful expression

$$u^t[(\epsilon + p)/u^t]_{,x^a} - \epsilon_{,x^a} + (\epsilon + p)u^t u_\phi \Omega_{,x^a} = 0. \tag{7c}$$

We note that

$$u^t = e^{-\nu}(1 - v^2)^{-1/2}, \quad u_\phi = r \sin \theta B e^{-\nu} v (1 - v^2)^{-1/2}. \tag{7d}$$

c) The Behavior of the Metric Potentials at $r = 0$, the Axis of Symmetry, and Large Radii

For a well behaved solution, the metric potentials ν, ω, B , and ζ have vanishing radial derivatives at $r = 0$ and have vanishing gradients perpendicular to the axis of symmetry. In addition, local flatness requires that

$$e^t = B \tag{8}$$

on the axis. Further, the condition of asymptotic flatness implies that the metric potentials have particular expansions in powers of $1/r$ at large radii, which we shall use to impose boundary conditions.

To obtain the asymptotic expansions for ν, ω , and B , we first write down the angular expansions

$$\nu = \sum_{l=0}^{\infty} \nu_{2l}(r) P_{2l}(\mu), \tag{9a}$$

$$\omega = \sum_{l=0}^{\infty} \omega_{2l}(r) P_{2l+1,\mu}(\mu), \tag{9b}$$

and

$$B = \sum_{l=0}^{\infty} B_{2l}(r) T_{2l}^{1/2}(\mu), \tag{9c}$$

where $\mu = \cos \theta$, $P_l(\mu)$ is a Legendre polynomial, and

$$T_l^{1/2}(\mu) = \frac{(-1)^l \Gamma(l+2)}{2^{l+1/2} l! \Gamma(l+\frac{3}{2})} (1-\mu^2)^{-1/2} \frac{d^l}{d\mu^l} (1-\mu^2)^{l+1/2} \quad (10a)$$

is a Gegenbauer polynomial (Morse and Feshbach 1953) satisfying

$$(1-\mu^2)T_l^{1/2}{}_{,\mu\mu} - 3\mu T_l^{1/2}{}_{,\mu} = -l(l+2)T_l^{1/2}, \quad (10b)$$

$$\int_{-1}^{+1} d\mu (1-\mu^2)^{1/2} T_l^{1/2}(\mu) T_m^{1/2}(\mu) = 1 \quad \text{if } l = m \\ = 0 \quad \text{if } l \neq m. \quad (10c)$$

The particular forms of the angular expansions (9) are useful because P_l , $P_{l,\mu}$, and $T_l^{1/2}$ are eigenfunctions of the angular parts of the operators $\mathbf{D} \cdot \mathbf{D}$, $\mathbf{D} \cdot \mathbf{r} \sin \theta \mathbf{D}$, and $\mathbf{D} \cdot \mathbf{r}^2 \sin^2 \theta \mathbf{D}$, respectively, that appear on the left-hand sides of equations (4a)–(4c). We next assume that the radial coefficients in equations (9) have expansions in powers of $1/r$ at large r with leading terms given by

$$v \sim -M/r, \quad (11a)$$

$$\omega \sim 2J/r, \quad (11b)$$

and

$$B \sim 1, \quad (11c)$$

where M is the total mass-energy of a model and J is its angular momentum. Substituting equations (9)–(11) into the field equations (4a)–(4c), we grind away and, before giving up, find

$$v \sim \left\{ -\frac{M}{r} + \frac{1}{3} \tilde{B}_0 \frac{M}{r^3} + \frac{J^2}{r^4} + \left[-\frac{1}{5} \tilde{B}_0^2 + \frac{1}{15} \tilde{B}_2 - \frac{12}{5} J^2 \right] \frac{M}{r^5} + \dots \right\} \\ + \left\{ \frac{\tilde{v}_2}{r^3} - 2 \frac{J^2}{r^4} + \left[-\frac{3}{7} \tilde{B}_0 \tilde{v}_2 + \frac{16}{21} \tilde{B}_2 M + \frac{24}{7} J^2 M \right] \frac{1}{r^5} + \dots \right\} P_2(\mu) + \left\{ \frac{\tilde{v}_4}{r^5} + \dots \right\} P_4(\mu) + \dots, \quad (12a)$$

$$\omega \sim \left\{ \frac{2J}{r^3} - \frac{6JM}{r^4} + \frac{6}{5} \left[8 - 3 \frac{\tilde{B}_0}{M^2} \right] \frac{JM^2}{r^5} + \left(\frac{40}{3} \tilde{B}_0 M - \frac{32}{3} M^3 - \frac{4}{5} \tilde{v}_2 \right) \frac{J}{r^6} \right. \\ + \left. \left(\frac{18}{35} \tilde{B}_2 + \frac{36}{7} \tilde{B}_0^2 + \frac{24}{5} J^2 - \frac{176}{7} \tilde{B}_0 M^2 + \frac{64}{7} M^4 + \frac{96}{35} \tilde{v}_2 M \right) \frac{J}{r^7} + \dots \right\} \frac{dP_1(\mu)}{d\mu} \\ + \left\{ \frac{\tilde{\omega}_2}{r^5} + \left(\frac{9}{5} \tilde{v}_2 J - \frac{5}{2} \tilde{\omega}_2 M \right) \frac{1}{r^6} - \left[\frac{96}{45} \tilde{B}_2 J + \frac{28}{5} \tilde{v}_2 J M + \frac{96}{45} J^3 + \frac{15}{9} \tilde{B}_0 \tilde{\omega}_2 - \frac{10}{3} \tilde{\omega}_2 M^2 \right] \frac{1}{r^7} + \dots \right\} \\ \times \frac{dP_3(\mu)}{d\mu} + \left\{ \frac{\tilde{\omega}_4}{r^7} + \dots \right\} \frac{dP_5(\mu)}{d\mu} + \dots, \quad (12b)$$

$$B \sim \left(\frac{\pi}{2} \right)^{1/2} \left(1 + \frac{\tilde{B}_0}{r^2} \right) T_0^{1/2}(\mu) + \left(\frac{\pi}{2} \right)^{1/2} \frac{\tilde{B}_2}{r^4} T_2^{1/2}(\mu) + \left(\frac{\pi}{2} \right)^{1/2} \frac{\tilde{B}_4}{r^6} T_4^{1/2}(\mu) + \dots \quad (12c)$$

In these equations, the constants M , J , \tilde{v}_{2l} , \tilde{B}_{2l} , and $\tilde{\omega}_{2l}$ are analogues of Newtonian multipole moments. Like Newtonian moments, the total mass-energy M and the angular momentum J can be evaluated in terms of integrals extending only over the matter distribution:

$$M = \int (-2T_t^t + T_a^a)(-g)^{1/2} dr d\theta d\varphi \\ = \int \left\{ B e^{2\zeta - 2\nu} \left[\frac{(\epsilon + p)(1 + v^2)}{1 - v^2} + 2p \right] + 2r \sin \theta \omega B^2 e^{2\zeta - 4\nu} \frac{(\epsilon + p)v}{1 - v^2} \right\} r^2 \sin \theta dr d\theta d\varphi, \quad (13)$$

$$J = \int_{\text{space-like 3-surface}} T_{ab} \gamma^b dS^a \\ = \int B^2 e^{2\zeta - 4\nu} \frac{(\epsilon + p)v}{1 - v^2} r^3 \sin^2 \theta dr d\theta d\varphi, \quad (14)$$

where g is the determinant of the metric tensor. The moments \tilde{v}_{2l} and $\tilde{\omega}_{2l}$, however, *cannot* be evaluated in such a way. This is because the exterior geometry acts explicitly as a source for these moments and it complicates the process of obtaining solutions. The moments \tilde{B}_{2l} *can* be evaluated in terms of integrals extending only over the interior of the fluid. Equations (4c), (10c), and (12c) imply that

$$\tilde{B}_{2l} = -16\pi(2/\pi)^{1/2}(4l+2)^{-1}r^{-(2l+2)} \int B' e^{2\zeta'} r'^{2l+3} (1-\mu'^2)^{1/2} T_{2l}^{1/2} dr' d\mu'. \quad (15)$$

d) Equations of State, Rotation Laws, and Integrated Forms of the Equations of Motion

In order to construct explicit equilibrium models, one must provide (i) equations of state

$$p = p(n, s, Z_i), \quad \epsilon = \epsilon(n, s, Z_i), \quad (16)$$

where n is the number density of baryons, s is the entropy per baryon, and Z_i are the fractional abundances of the different nuclear species; (ii) instructions for determining essentially the distributions of s and Z_i throughout the fluid; and (iii) instructions (the rotation law) for determining the distribution of angular velocity Ω or of the angular momentum per baryon,

$$j = \frac{(\epsilon + p)}{n} u_\phi. \quad (17)$$

In this series of papers, we shall be especially interested in choices of equations of state and rotation laws that enable us to directly integrate the equations of motion (7c). A couple of examples of what we have in mind here are the following.

Suppose, in a first example, that the distributions of entropy $s(x^\alpha)$ and of the fractional abundance $Z_i(x^\alpha)$ are determined uniquely by the distribution of baryons $n(x^\alpha)$. Then equations (16) yield equations of state of the baryotropic form

$$\epsilon = \epsilon(p), \quad n = n(p), \quad (18)$$

and the integrability condition for the equations of motion (7c) is the rotation law

$$u_\phi u^t \equiv j/\Phi = F(\Omega), \quad (19)$$

where $F(\Omega)$ is a specifiable function of Ω and

$$\Phi \equiv (\epsilon + p)/(nu^t) \quad (20)$$

is the so-called injection energy, i.e., the energy required to inject a zero-angular-momentum baryon from infinity into the star. In the Newtonian limit $u_\phi u^t \rightarrow (r \sin \theta)^2 \Omega$, so that equation (19) is the relativistic generalization of the Newtonian statement that the angular velocity is constant on cylinders when the equations of state are baryotropic. In the present example, the equations of motion (7c) integrate to the form

$$\ln(1/u^t) + \int_0^p dp' / (\epsilon' + p') - \int_\Omega^{\Omega_A} F(\Omega') d\Omega' = \ln \beta^{1/2}, \quad (21)$$

where Ω_A is the constant value of Ω on the symmetry axis and β is the value of $e^{2\nu}$ at the pole of the star. Note that equations (6), (8c), (19), and (21) determine p (and hence ϵ) and Ω in terms of Ω_A , β , and the metric potentials. Hence specification of equations of state, $F(\Omega)$, Ω_A , and β determine a unique model (assuming it exists). A special rotation law is that of uniform rotation,

$$\Omega = \text{constant}. \quad (22)$$

When the law (19) is specialized to (22), equation (21) is specialized to

$$\ln(1/u^t) + \int_0^p dp' / (\epsilon' + p') = \ln \beta^{1/2}. \quad (23)$$

A chosen constant value of Ω and equation (23) determine p uniquely in terms of the metric functions.

Now suppose, in a second example, that the configuration is isentropic ($s = \text{constant}$) and the Z_i either are constant or are determined uniquely by the baryon density n . Suppose further that the rotation law is of the form

$$j = F(\Omega). \quad (24)$$

Then equations of the form (18) are again valid, and equation (8b) integrates to

$$\Phi - \int_{\Omega}^{\Omega_A} F(\Omega') d\Omega' = \mu_B \beta^{1/2}, \quad (25)$$

where Ω_A and β are defined as before and μ_B is the rest mass per baryon. In this example also, specification of equations of state, $F(\Omega)$, Ω_A , and β determine a unique model (assuming it exists).

III. THE METHOD OF SOLVING THE STRUCTURE EQUATIONS

a) An Outline of the Method

Our method of constructing models is a generalization of Stoeckly's (1965) Newtonian method. First an initial approximation $\nu, \omega, B, \zeta, \Omega, p$ to a solution is obtained in one way or another. This approximation is imagined to differ by small amounts $\delta\nu, \delta\omega, \dots$, from the desired solution. Equation (4a) is expanded to first order in $\delta\nu$, and a Poisson-like linear partial differential equation for $\delta\nu$ is obtained, with source terms that involve only the initial approximation ν, ω, \dots , and that are nonvanishing for all $r < \infty$. This linearized equation and another one obtained by imposing boundary conditions in a way explained below are replaced by difference equations on a finite grid in the (r, θ) -plane. The difference equations are then solved for the values of $\delta\nu$ at the grid points, and ν is replaced by $\nu + \delta\nu$ in the approximate solution. Next the chosen equations of state, rotation law, and integrated equations of motion are used to obtain new distributions of angular velocity and matter. After this, similar procedures, involving recomputation of Ω and p at each stage, are followed to obtain new approximations for ω, B , and ζ . All of the above steps are iterated until (hopefully) convergence is achieved and the changes in quantities at the grid points drop below some desired upper limit.

b) The Linearized Versions of the Field Equations and of the Asymptotic Boundary Conditions

One obtains the linearized field equations for $\delta\nu$ by replacing ν in equation (4a) with $\nu + \delta\nu$ and expanding to first order in $\delta\nu$. The result is

$$\begin{aligned} B\delta\nu_{,rr} + \left(2\frac{B}{r} + B_{,r}\right)\delta\nu_{,r} + \frac{B}{r^2} D_{\mu}^2 \delta\nu + \frac{(1-\mu^2)}{r^2} B_{,\mu} \delta\nu_{,\mu} \\ + \left[2(1-\mu^2)r^2 B^3 e^{-4\nu} \left[(\omega_{,r})^2 + \frac{(1-\mu^2)}{r^2} (\omega_{,\mu})^2 \right] - 4\pi B e^{2\zeta} \frac{\partial}{\partial\nu} \left\{ e^{-2\nu} \left[\frac{(\epsilon+p)(1+v^2)}{1-v^2} + 2p \right] \right\} \right] \delta\nu \\ = -B\nu_{,rr} - \left(2\frac{B}{r} + B_{,r}\right)\nu_{,r} - \frac{B}{r^2} D_{\mu}^2 \nu - \frac{(1-\mu^2)}{r^2} B_{,\mu} \nu_{,\mu} + \frac{1}{2}(1-\mu^2)r^2 B^3 e^{-4\nu} \\ \times [(\omega_{,r})^2 + (1-\mu^2)r^{-2}(\omega_{,\mu})^2] + 4\pi B e^{2\zeta-2\nu} \left[\frac{(\epsilon+p)(1+v^2)}{1-v^2} + 2p \right], \quad (26) \end{aligned}$$

where

$$\mu \equiv \cos \theta \quad (27)$$

and

$$D_{\mu}^2 f \equiv (\partial/\partial\mu)[(1-\mu^2)\partial f/\partial\mu]. \quad (28)$$

Certain terms on the left-hand side of equation (24) arise from the changes in ϵ, p , and v that are associated with a change $\delta\nu$ in ν . For the examples of § II d, these terms are determined by equation (6), the equation of state (18) the rotation law (19), (21), or (23), and the integrated equations of motion (21), (23), or (25). It turns out that the inclusion, or "relaxation," of these matter terms is crucial to the successful convergence of our iterative method of solution. One obtains the linearized field equations for $\delta\omega$ and δB from equations (4b) and (4c). The results are

$$\begin{aligned} \delta\omega_{,rr} + \left(\frac{4}{r} + \frac{3}{B} B_{,r} - 4\nu_{,r}\right)\delta\omega_{,r} + \frac{1}{r^2} D_{\mu}^2 \delta\omega \\ - \left[2\mu - (1-\mu^2) \left(\frac{3}{B} B_{,\mu} - 4\nu_{,\mu}\right) \right] \frac{\delta\omega_{,\mu}}{r^2} + 16\pi e^{2\zeta-2\nu} \frac{\partial}{\partial\omega} \left[\frac{(\epsilon+p)(\Omega-\omega)}{1-v^2} \right] \delta\omega \\ = -\omega_{,rr} - \left(\frac{4}{r} + \frac{3}{B} B_{,r} - 4\nu_{,r}\right)\omega_{,r} - \frac{1}{r^2} D_{\mu}^2 \omega \\ + \left[2\mu - (1-\mu^2) \left(\frac{3}{B} B_{,\mu} - 4\nu_{,\mu}\right) \right] \frac{\omega_{,\mu}}{r^2} - 16\pi e^{2\zeta-2\nu} \frac{(\epsilon+p)(\Omega-\omega)}{1-v^2}, \quad (29) \end{aligned}$$

$$\begin{aligned} \delta B_{,rr} + \frac{3}{r} \delta B_{,r} + \frac{1}{r^2} D_\mu^2 \delta B - \frac{\mu}{r^2} \delta B_{,\mu} - 16\pi e^{2\zeta-2\nu} \frac{\partial}{\partial B} (Bp) \delta B \\ = -B_{,rr} - \frac{3}{r} B_{,r} - \frac{1}{r^2} D_\mu^2 B + \frac{\mu}{r^2} B_{,\mu} + 16\pi B e^{2\zeta-2\nu} p. \end{aligned} \quad (30)$$

Equation (4d) is already linear in ζ , and we shall use it (and eq. [8]) in unaltered form to find ζ in terms of the other metric potentials.

In order to solve equations (26), (29), and (30), one must impose, in particular, the boundary conditions (12a)–(12c) associated with asymptotic flatness. There is a problem involved in imposing the conditions (12a) and (12b) at some finite value of r . It involves the fact that, as we mentioned, the “multipoles” $\tilde{\nu}_{2l}$ and $\tilde{\omega}_{2l}$ ($l \geq 1$) cannot be expressed in terms of integrals extending only over the matter distribution. Wilson (1972) ignored this fact and, carrying the expansions for ν and ω only to $O(r^{-3})$, chose to approximate ν_2 by a Newtonian-like integral extending only over the fluid and selected in an ad hoc manner. The accuracy of such a way of imposing boundary conditions might be questioned, at least in highly relativistic situations.

Our method essentially lets the computer decide on the values of the multipole moments in a manner that is entirely consistent with the field equations. We achieve this by reformulating the boundary conditions (12) in a certain way. We focus first on the metric function ν . Recall the angular expansion

$$\nu(r, \mu) = \sum_{l=0}^{\infty} \nu_{2l}(r) P_{2l}(\mu) \quad (31)$$

and the expansion (12a) for the ν_{2l} in powers of $1/r$. For reasons that will become clear, we seek an expression which, like (12a), states that ν falls off as a power series in $1/r$, but in which the constants $\tilde{\nu}_{2l}$ have been eliminated in favor of the $\nu_{2l}(r)$. We obtain the desired form and its linearized version by taking the derivative

$$\nu_{,r}(r, \mu) = \sum_{l=0}^{\infty} \nu_{2l,r}(r) P_{2l}(\mu) \quad (32)$$

and using the facts that, to $O[(M/r)^5]$,

$$\nu_{0,r}(r) \approx -\frac{\nu_0(r)}{r} - \frac{2}{3} \tilde{B}_0 \frac{M}{r^4} - 3 \frac{J^2}{r^5} + \left[\frac{4}{5} \tilde{B}_0^2 - \frac{4}{15} \tilde{B}_2 + \frac{48}{5} J^2 \right] \frac{M}{r^6}, \quad (33a)$$

$$\nu_{2,r}(r) \approx \left[-3 + \frac{6}{7} \frac{\tilde{B}_0}{r^2} \right] \frac{\nu_2(r)}{r} + 2 \frac{J^2}{r^5} - \frac{16}{7} \left(\frac{2}{3} \tilde{B}_2 + 3J^2 \right) \frac{M}{r^6}, \quad (33b)$$

$$\nu_{2l,r}(r) \approx -(2l+1) \frac{\nu_{2l}(r)}{r} \quad \text{for } l \geq 2. \quad (33c)$$

Combining equations (32) and (33), and linearizing, we have

$$\begin{aligned} \delta \nu_{,r}(r, \mu) + \sum_{l=0}^{\infty} \frac{(2l+1)}{r} \delta \nu_{2l}(r) P_{2l}(\mu) - \frac{6}{7} \frac{\tilde{B}_0}{r^3} \delta \nu_2(r) P_2(\mu) \\ \approx -\nu_{,r}(r, \mu) - \sum_{l=0}^{\infty} \frac{(2l+1)}{r} \nu_{2l}(r) P_{2l}(\mu) - \left[\frac{2}{3} \tilde{B}_0 \frac{M}{r^4} + 3 \frac{J^2}{r^5} - \left(\frac{4}{5} \tilde{B}_0^2 - \frac{4}{15} \tilde{B}_2 + \frac{48}{5} J^2 \right) \frac{M}{r^6} \right] \\ + \left[\frac{6}{7} \frac{\tilde{B}_0}{r^3} \nu_2(r) + 2 \frac{J^2}{r^5} - \left(\frac{32}{21} \tilde{B}_2 + \frac{48}{7} J^2 \right) \frac{M}{r^6} \right] P_2(\mu), \end{aligned} \quad (34a)$$

where it is to be noted that

$$\nu_{2l}(r) = \frac{1}{2}(4l+1) \int_{-1}^{+1} d\mu \nu(r, \mu) P_{2l}(\mu). \quad (34b)$$

This is the desired linearized form of the boundary condition for ν . As we shall see, once a grid of points has been set up in the (r, θ) -plane, the $\nu_{2l}(r)$ can be approximated by a linear combination of the values of ν at the various grid points. This boundary condition can then be imposed in the same way, involving the difference-equation approximations spelled out below, as the linearized field equations.

We obtain the linearized version of the boundary condition for ω in a similar manner. If, for convenience, we define quantities $\omega_{2l}^\dagger(r)$ by

$$\omega(r, \mu) \equiv \sum_{l=0}^{\infty} \omega_{2l}^\dagger(r) P_{2l}(\mu), \quad (35)$$

then

$$\begin{aligned} \omega_0^\dagger(r) = & \frac{2J}{r^3} - \frac{6JM}{r^4} + \left[\frac{48}{5} JM^2 - \frac{18}{5} J\tilde{B}_0 + \tilde{\omega}_2 \right] \frac{1}{r^5} + \left[\frac{40}{3} J\tilde{B}_0 M - \frac{32}{3} JM^3 + J\tilde{v}_2 - \frac{5}{2} M\tilde{\omega}_2 \right] \frac{1}{r^6} \\ & + \left[-\frac{34}{21} J\tilde{B}_2 + \frac{36}{7} J\tilde{B}_0^2 + \frac{8}{3} J^3 - \frac{176}{7} J\tilde{B}_0 M^2 + \frac{64}{7} JM^4 - \frac{20}{7} JM\tilde{v}_2 \right. \\ & \left. - \left(\frac{5}{3} \tilde{B}_0 - \frac{10}{3} M^2 \right) \tilde{\omega}_2 + \tilde{\omega}_4 \right] \frac{1}{r^7} + \dots, \end{aligned} \quad (36a)$$

$$\tilde{\omega}_2^\dagger(r) = \frac{5\tilde{\omega}_2}{r^5} + \left(9J\tilde{v}_2 - \frac{25}{2} M\tilde{\omega}_2 \right) \frac{1}{r^6} - \left[\frac{32}{3} J\tilde{B}_2 + \frac{32}{3} J^3 + 28JM\tilde{v}_2 + \frac{25}{3} (\tilde{B}_0 - 2M^2)\tilde{\omega}_2 - 5\tilde{\omega}_4 \right] \frac{1}{r^7} + \dots, \quad (36b)$$

$$\tilde{\omega}_4^\dagger(r) = \frac{9\tilde{\omega}_4}{r^7} + \dots, \quad (36c)$$

and so on. The linearized boundary condition for ω becomes

$$\begin{aligned} \delta\omega_{,r}(r, \mu) + \sum_{i=0}^{2l+3} \frac{(2l+3)}{r} \delta\omega_{2i}^\dagger(r) P_{2i}(\mu) - \left\{ -\frac{2}{5r} + \frac{1}{2} \frac{M}{r^2} + \left(\frac{2}{3} \tilde{B}_0 - \frac{1}{12} M^2 \right) \frac{1}{r^3} \right. \\ \left. + \left[\frac{5}{2} \frac{M}{r^2} - \left(\frac{5}{12} M^2 - \frac{10}{3} \tilde{B}_0 \right) \frac{1}{r^3} \right] P_2(\mu) \right\} \delta\omega_2^\dagger(r) + \frac{2}{9} [1 + 5P_2(\mu)] \frac{\delta\omega_4^\dagger(r)}{r} \\ \approx -\omega_{,r}(r, \mu) - \sum_{i=0}^{2l+3} \frac{(2l+3)}{r} \omega_{2i}^\dagger(r) P_{2i}(\mu) \\ + \left\{ -\frac{2}{5r} + \frac{1}{2} \frac{M}{r^2} + \left(\frac{2}{3} \tilde{B}_0 - \frac{1}{12} M^2 \right) \frac{1}{r^3} + \left[\frac{5}{2} \frac{M}{r^2} - \left(\frac{5}{12} M^2 - \frac{10}{3} \tilde{B}_0 \right) \frac{1}{r^3} \right] P_2(\mu) \right\} \omega_2^\dagger(r) \\ - \frac{2}{9} [1 + 5P_2(\mu)] \frac{\omega_4^\dagger(r)}{r} + 6J \frac{M}{r^5} - \frac{12}{5} (8M^2 - 3\tilde{B}_0) \frac{J}{r^6} + 8(4M^2 - 5\tilde{B}_0) \frac{JM}{r^7} \\ + \left[-\frac{144}{7} \tilde{B}_0^2 + \frac{704}{7} \tilde{B}_0 M^2 - \frac{256}{7} M^4 - \frac{206}{15} J^2 + \frac{232}{105} \tilde{B}_2 + \frac{2}{3} (32\tilde{B}_2 + 5J^2) P_2(\mu) \right] \frac{J}{r^8} \\ + \left[\frac{3}{10} - \frac{129}{84} \frac{M}{r} - \left(\frac{9}{2} - \frac{31}{4} \frac{M}{r} \right) P_2(\mu) \right] \frac{J}{r^4} N_2(r), \end{aligned} \quad (37a)$$

where

$$N_2(r) \equiv 2(1 - 2M/r)v_2(r). \quad (37b)$$

Although equation (15) shows that coefficients B_{2i} in the boundary condition (12c) for B can be evaluated directly by an integral over the matter distribution, we shall treat (12c) in the same way as we treat (12a) and (12b). Thus, defining the quantities $B_{2i}^\dagger(r)$ by

$$B(r, \mu) \equiv \sum_{i=0}^{2l} B_{2i}^\dagger(r) P_{2i}(\mu), \quad (38)$$

we have

$$B_0^\dagger(r) = 1 + \left(\frac{\tilde{B}_0}{r^2} + \frac{1}{3} \frac{\tilde{B}_2}{r^4} + \frac{7}{35} \frac{\tilde{B}_4}{r^6} \right) + \dots, \quad (39a)$$

$$B_2^\dagger(r) = 8 \left(\frac{1}{3} \frac{\tilde{B}_2}{r^4} + \frac{1}{7} \frac{\tilde{B}_4}{r^6} \right) + \dots, \quad (39b)$$

$$B_4^\dagger(r) = \frac{128}{35} \frac{\tilde{B}_4}{r^6} + \dots, \quad (39c)$$

and so on. The linearized boundary condition for B becomes

$$\begin{aligned} \delta B_{,r}(r, \mu) + \sum_{i=0} \frac{(2l+2)}{r} \delta B_{2i}^{\dagger}(r) P_{2i}(\mu) + \frac{1}{4} \frac{\delta B_2^{\dagger}(r)}{r} + \frac{3}{16} \left[\frac{3}{4} + \frac{10}{3} P_2(\mu) \right] \frac{\delta B_4^{\dagger}(r)}{r} \\ \approx \frac{2}{r} - \sum_{i=0} \frac{(2l+2)}{r} B_{2i}^{\dagger}(r) P_{2i}(\mu) - \frac{1}{4} \frac{B_2^{\dagger}(r)}{r} - \frac{3}{16} \left[\frac{3}{4} + \frac{10}{3} P_2(\mu) \right] \frac{B_4^{\dagger}(r)}{r}. \end{aligned} \quad (40)$$

c) *The Difference Equations and the Procedure for Solving Them*

In our method we approximate the linearized equations by difference equations on a finite grid in the (r, θ) -plane. The metric functions are assumed to be even functions of μ , so a grid covering the range $0 \leq \mu \leq 1$ will suffice. Our grid is that of Stoeckly (1965). It consists of a chosen number, L , of radial spokes emanating from the origin at the Gauss-Legendre quadrature values $\mu_1 = 0, \mu_2, \dots, \mu_L$ of μ associated with the integer L (see, e.g., Kopal 1961). A chosen number, I , of grid points are uniformly spaced at chosen radial intervals Δr along each spoke. (The outermost grid points should ideally always lie far outside the stellar surface.) The coordinates of a particular grid point are $r = h\Delta r, \mu = \mu_i$, where $1 \leq h \leq I$, and $1 \leq i \leq L$.

The difference equations result from approximating r and μ derivatives—we shall always assume that a function of μ is even in μ unless noted otherwise—by certain linear combinations of the function's values at various grid points.

Consider first the approximation of μ derivatives. Following Stoeckly (1965), assume that a function f is approximated with sufficient accuracy by the expansion

$$f(r, \mu) \approx \sum_{l'=0}^{L-1} f_{2l'}(r) P_{2l'}(\mu). \quad (41)$$

Each radial function has the Gauss-Legendre quadrature approximation

$$\begin{aligned} f_{2l'}(r) &= \frac{1}{2}(4l' + 1) \int_{-1}^{+1} d\mu f(r, \mu) P_{2l'}(\mu) \\ &\approx \frac{1}{2}(4l' + 1) \sum_{m=1}^L H_m f(r, \mu_m) P_{2l'}(\mu_m). \end{aligned} \quad (42)$$

Here the weighting functions H_m , for $m \geq 2$, are to be assigned twice their usual values, since only quadrature points at nonnegative μ are used. The approximation (42) becomes exact when the integrand $f(r, \mu) P_{2l'}(\mu)$ is an even polynomial in μ of degree $\leq 2(2l' - 1) - 2$. Hence (42) is exact for $0 \leq l' \leq L - 1$ if $f(r, \mu)$ is an even polynomial in μ of degree $\leq 2L - 2$, i.e. if equation (41) is exact. Equations (28), (42), and the derivatives of (41) yield the desired approximations

$$f_{, \mu}(r, \mu_i) \approx \sum_{m=1}^L F_{im} f(r, \mu_m), \quad (43a)$$

$$F_{im} \equiv \sum_{l'=1}^{L-1} \frac{1}{2}(4l' + 1) H_m P_{2l', \mu}(\mu_i) P_{2l'}(\mu_m), \quad (43b)$$

$$D_{\mu}^2 f(r, \mu_i) = \sum_{m=1}^L G_{im} f(r, \mu_m), \quad (44a)$$

$$G_{im} \equiv - \sum_{l'=1}^{L-1} l'(2l' + 1)(4l' + 1) H_m P_{2l'}(\mu_i) P_{2l'}(\mu_m). \quad (44b)$$

Turn now to the approximation of radial derivatives, the explicit forms of the difference equations, and the procedure for obtaining solutions. There are two different cases here, and we consider them separately.

i) *The Case for Which the Density Drops Smoothly to Zero at the Stellar Surface*

Here every quantity of interest is at least $C^{(2)}$ everywhere; and the basic way chosen to approximate a radial derivative is to fit the usual sort of Lagrangian polynomial to a quantity and then to differentiate the polynomial.

One such way to approximate radial derivatives by forward difference formulae when $h = 1$ and central formulae when $2 \leq h \leq I - 1$ (it turns out that derivatives at $h = I$ are not required) is this:

$$h = 1$$

$$f_{,r}(\Delta r, \mu_l) \approx (1/6\Delta r)(-11 f_{1,l} + 18f_{2,l} - 9f_{3,l} + 2f_{4,l}), \quad (45a)$$

$$f_{,rr}(\Delta r, \mu_l) \approx (1/\Delta r^2)(2f_{1,l} - 5f_{2,l} + 4f_{3,l} - f_{4,l}), \quad (45b)$$

where we have introduced the notation

$$f_{h,l} \equiv f(h\Delta r, \mu_l). \quad (46)$$

(Recall that a comma subscript denotes a derivative only when followed by a coordinate symbol.)

$$2 \leq h \leq I - 1$$

$$f_{,r}(h\Delta r, \mu_l) \approx (1/2\Delta r)(-f_{h-1,l} + f_{h+1,l}), \quad (47a)$$

$$f_{,rr}(h\Delta r, \mu_l) \approx (1/\Delta r^2)(f_{h-1,l} - 2f_{h,l} + f_{h+1,l}). \quad (47b)$$

It is now straightforward to combine equations (26), (34), and (42)–(47) to obtain difference equations for $\delta\nu_{h,l}$ when $1 \leq h \leq I$, $\mu_1 \leq \mu_l \leq \mu_L$. Defining

$$a \equiv B/h + \frac{1}{2}\Delta r B_{,r} \quad (48)$$

and

$$\text{RHS}(\nu) \equiv \Delta r^2 \times (\text{right side of eq. [26]}), \quad (49)$$

we find the following for various values of h :

$$h = 1, r = \Delta r, \mu = \mu_l$$

$$\left[\left(2B - \frac{22}{6}a \right) + 2(1 - \mu^2)r^2 B^3 e^{-4\nu} \Delta r^2 \mathbf{D}\omega \cdot \mathbf{D}\omega - 4\pi B e^{2\zeta} \frac{\partial}{\partial \nu} \left\{ e^{-2\nu} \left[\frac{(\epsilon + p)(1 + v^2)}{1 - v^2} + 2p \right] \right\} \right] \delta\nu_{1,l} \\ + \sum_m [BG_{1m} + (1 - \mu^2)B_{,\mu}F_{1m}] \delta\nu_{1,m} - (5B - 6a)\delta\nu_{2,l} + (4B - 3a)\delta\nu_{3,l} - (B - \frac{2}{3}a)\delta\nu_{4,l} = \text{RHS}(\nu). \quad (50a)$$

$$2 \leq h \leq I - 1, r = h\Delta r, \mu = \mu_l$$

$$(B - a)\delta\nu_{h-1,l} + \left[-2B + 2(1 - \mu^2)r^2 B^3 e^{-4\nu} \Delta r^2 \mathbf{D}\omega \cdot \mathbf{D}\omega - 4\pi B e^{2\zeta} \frac{\partial}{\partial \nu} \left\{ e^{-2\nu} \left[\frac{(\epsilon + p)(1 + v^2)}{1 - v^2} + 2p \right] \right\} \right] \delta\nu_{h,l} \\ + \frac{1}{h^2} \sum_m [BG_{hm} + (1 - \mu^2)B_{,\mu}F_{hm}] \delta\nu_{h,m} + (B + a)\delta\nu_{h+1,l} = \text{RHS}(\nu). \quad (50b)$$

$$h = I - 1, r = h\Delta r, \mu = \mu_l$$

$$-\frac{1}{2}\delta\nu_{h-1,l} + \frac{1}{h} \sum_m \tilde{C}_{1m} \delta\nu_{h,m} + \frac{1}{2}\delta\nu_{h+1,l} = -\Delta r \nu_{,r} - \frac{1}{h} \sum_m \tilde{C}_{1m} \nu_{h,m} \\ - \Delta r \left[\frac{2}{3} \tilde{B}_0 \frac{M}{r^4} + 3 \frac{J^2}{r^5} - \frac{1}{5} \left(4\tilde{B}_0^2 - \frac{4}{3} \tilde{B}_2 + 48J^2 \right) \frac{M}{r^6} \right] \\ + 2\Delta r \left[\frac{J^2}{r^5} - \left(\frac{16}{21} \tilde{B}_2 + \frac{24}{7} J^2 \right) \frac{M}{r^6} \right] P_2(\mu_l), \quad (50c)$$

where

$$\tilde{C}_{1m} \equiv H_m \sum_{l'=0}^{L-1} \frac{1}{2} (2l' + 1)(4l' + 1) P_{2l'}(\mu_l) P_{2l'}(\mu_m) - \frac{15}{7} H_m \frac{\tilde{B}_0}{r^2} P_2(\mu_l) P_2(\mu_m). \quad (50d)$$

In these equations, derivatives of ν , B , and ω are understood to be approximated by the same formulae used to approximate derivatives of $\delta\nu$.

Equations (50) provide $I \times L$ coupled equations for the $I \times L$ quantities $\delta\nu_{h,i}$. We should note that $\epsilon = p = 0$ for grid points lying outside the guessed location of the surface. This effectively takes care of the boundary condition at the surface. Concerning the demand that the solution be well behaved at $r = 0$, it turns out that, just as Stoeckly noticed in his Newtonian calculations, an explicit boundary condition is not needed at $r = 0$. (In fact, we have not even placed a grid point at $r = 0$.) The reason appears to be this: the approximation of ν by a Lagrangian polynomial fitted to the grid-point values of ν implies that ν is finite at $r = 0$ if it is finite at the various grid points; hence the scheme implicitly picks out the well-behaved solution near $r = 0$.

The equations for the $\delta\omega_{h,i}$ come from equations (29), (35), (37), and (41)–(47). Defining

$$b \equiv 4/h + 3B^{-1}\Delta r B_r - 4\Delta r\nu_r \quad (51)$$

and

$$\text{RHS}(\omega) \equiv \Delta r^2 \times (\text{right side of eq. [29]}), \quad (52)$$

we find the following:

$$\begin{aligned} & \underline{h = 1, r = \Delta r, \mu = \mu_i} \\ & \left\{ \left(2 - \frac{11}{6}b \right) + 16\pi\Delta r^2 e^{2\zeta - 2\nu} \frac{\partial}{\partial \omega} \left[\frac{(\epsilon + p)(\Omega - \omega)}{1 - v^2} \right] \right\} \delta\omega_{1,i} \\ & + \sum_m \{ G_{1m} + [-2\mu + (1 - \mu^2)(b - 4)] F_{1m} \} \delta\omega_{1,m} \\ & + (-5 + 3b)\delta\omega_{2,i} + \left(4 - \frac{3}{2}b \right) \delta\omega_{3,i} + \left(-1 + \frac{1}{3}b \right) \delta\omega_{4,i} = \text{RHS}(\omega). \quad (53a) \end{aligned}$$

$$\begin{aligned} & \underline{2 \leq h \leq I - 1, r = h\Delta r, \mu = \mu_i} \\ & \left(1 - \frac{1}{2}b \right) \delta\omega_{h-1,i} + \left\{ -2 + 16\pi\Delta r^2 e^{2\zeta - 2\nu} \frac{\partial}{\partial \omega} \left[\frac{(\epsilon + p)(\Omega - \omega)}{1 - v^2} \right] \right\} \delta\omega_{h,i} \\ & + \frac{1}{h^2} \sum_m \{ G_{hm} + [-2\mu + (1 - \mu^2)(b - 4)] F_{hm} \} \delta\omega_{h,m} + \left(1 + \frac{1}{2}b \right) \delta\omega_{h+1,i} = \text{RHS}(\omega). \quad (53b) \end{aligned}$$

$$\begin{aligned} & \underline{h = I - 1, r = h\Delta r, \mu = \mu_i} \\ & -\frac{1}{2} \delta\omega_{h-1,i} + \frac{1}{h} \sum_m \tilde{D}_{hm} \delta\omega_{h,m} + \frac{1}{2} \delta\omega_{h+1,i} \\ & = -\Delta r\omega_r - \frac{1}{h} \sum_m \tilde{D}_{hm}\omega_{h,m} \\ & + \Delta r \left\{ 6J \frac{M}{r^5} - \frac{12}{5} (8M^2 - 3\tilde{B}_0) \frac{J}{r^6} + 8(4M^2 - 5\tilde{B}_0) J \frac{M}{r^7} \right. \\ & + \left[-\frac{144}{7} \tilde{B}_0^2 + \frac{704}{7} \tilde{B}_0 M^2 - \frac{256}{7} M^4 - \frac{206}{15} J^2 + \frac{232}{105} \tilde{B}_2 + \frac{2}{3} (32\tilde{B}_2 + 5J^2) P_2(\mu) \right] \frac{J}{r^8} \\ & \left. + 5 \left[\frac{3}{10} - \frac{129}{84} \frac{M}{r} - \left(\frac{9}{2} - \frac{31}{4} \frac{M}{r} \right) P_2(\mu) \right] \left(1 - 2 \frac{M}{r} \right) \frac{J}{r^4} \sum_m [H_m \nu_{h,m} P_2(\mu_m)] \right\}, \quad (53c) \end{aligned}$$

where

$$\begin{aligned} \tilde{D}_{lm} & \equiv \sum_{l'=0}^{l-1} \frac{1}{2} (4l' + 1)(2l' + 3) H_m P_{2l'}(\mu_i) P_{2l'}(\mu_m) - \frac{5}{2} \left(-\frac{2}{5} + \frac{1}{2} \frac{M}{r} + \frac{2}{3} \frac{\tilde{B}_0}{r^2} - \frac{1}{12} \frac{M^2}{r^2} \right) H_m P_2(\mu_m) \\ & + H_m P_4(\mu_m) - \frac{25}{2} \left(\frac{1}{2} \frac{M}{r} - \frac{1}{12} \frac{M^2}{r^2} + \frac{2}{3} \frac{\tilde{B}_0}{r^2} \right) H_m P_2(\mu_i) P_2(\mu_m) + 5 H_m P_2(\mu_i) P_4(\mu_m). \quad (53d) \end{aligned}$$

One solves equations (53) to obtain a new guess $\omega + \delta\omega$.

The equations for the $\delta B_{h,i}$ come from equations (30), (38), (40), and (41)–(47). Defining

$$\text{RHS}(B) \equiv \Delta r^2 \times (\text{right-hand side of eq. [30]}), \quad (54)$$

we find the following:

$$\begin{aligned} & \underline{h = 1, r = \Delta r, \mu = \mu_l} \\ & - \left[\frac{7}{2} + 16\pi\Delta r^2 e^{2\zeta - 2\nu} \frac{\partial}{\partial B} (Bp) \right] \delta B_{1,l} + \sum_m (G_{lm} - \mu F_{lm}) \delta B_{1,m} + 4\delta B_{2,l} - \frac{1}{2} \delta B_{3,l} = \text{RHS}(B). \end{aligned} \quad (55a)$$

$$\begin{aligned} & \underline{2 \leq h \leq I - 1, r = h\Delta r, \mu = \mu_l} \\ & \left(1 - \frac{3}{2h} \right) \delta B_{h-1,l} - \left[2 + 16\pi\Delta r^2 e^{2\zeta - 2\nu} \frac{\partial}{\partial B} (Bp) \right] \delta B_{h,l} \\ & \quad + \frac{1}{h^2} \sum_m (G_{lm} - \mu F_{lm}) \delta B_{h,m} + \left(1 + \frac{3}{2h} \right) \delta B_{h+1,l} = \text{RHS}(B). \end{aligned} \quad (55b)$$

$$\begin{aligned} & \underline{h = I - 1, r = h\Delta r, \mu = \mu_l} \\ & -\frac{1}{2} \delta B_{h-1,l} + \frac{1}{h} \sum_m \tilde{E}_{lm} \delta B_{h,m} + \frac{1}{2} \delta B_{h+1,l} = -\Delta r B_{,r} + \frac{2}{h} - \frac{1}{h} \sum_m \tilde{E}_{lm} B_{h,m} \end{aligned} \quad (55c)$$

where

$$\tilde{E}_{lm} \equiv \sum_{l'=0}^{l-1} \frac{1}{2} (4l' + 1)(2l' + 2) H_m P_{2l'}(\mu_l) P_{2l'}(\mu_m) + \frac{5}{8} H_m P_2(\mu_m) + \frac{9}{16} \left[\frac{9}{8} + 5P_2(\mu_l) \right] H_m P_4(\mu_m). \quad (55d)$$

One solves equations (55) to obtain a new guess $B + \delta B$.

Equation (4d) is already linear in ζ , and we can use it along with the boundary condition (8) to find ζ at the grid points. One way to do this is to write, within our level of approximation,

$$\zeta_{,u} \approx \sum_{l'=1}^{L-1} \zeta_{2l'}(r) P_{2l',u}(\mu). \quad (56)$$

Equation (4d) gives an expression, odd in μ , for $\zeta_{,u}$. Combining it with (42), (57), and the orthonormality relations for the $P_{2l',u}$ yields

$$\zeta_{2l'}(r) \approx \frac{(4l' + 1)}{4l'(2l' + 1)} \sum_m H_m (1 - \mu_m^2) P_{2l',u}(\mu_m) \zeta_{,u}(r, \mu_m), \quad (57)$$

for $1 \leq l' \leq L - 1$; and hence

$$\zeta(r, \mu) \approx \zeta_0(r) + \sum_{l'=1}^{L-1} \frac{(4l' + 1)}{4l'(2l' + 1)} \left[\sum_{m=1}^L H_m (1 - \mu_m^2) P_{2l',u}(\mu_m) \zeta_{,u}(r, \mu_m) \right] P_{2l'}(\mu), \quad (58)$$

where $\zeta_0(r)$ is determined by the boundary condition that $\zeta = \ln B$ at $\mu = 1$.

A successful method for computing models with density distributions that drop smoothly to zero at the stellar surface is the following.

Fix, once and for all, the equations of state, the rotation law, Ω_A , and β (cf. § II d). Having obtained (e.g., by using a solution constructed for smaller Ω_A) a guess for ν , ω , B , ζ , Ω , and p , substitute that guess into equations (50), and solve for $\delta\nu_{h,l}$ by Gaussian-elimination techniques. Replace the $\nu_{h,l}$ with $\nu_{h,l} + \delta\nu_{h,l}$, and use either equations (19) and (21), (22) and (23), or (24) and (25) to obtain new $\Omega_{h,l}$ and $p_{h,l}$. Solve equations (53) to obtain new $\omega_{h,l}$, and recompute the $\Omega_{h,l}$ and $p_{h,l}$ as before. Solve equations (55) to obtain new $B_{h,l}$, use (58) to obtain new $\zeta_{h,l}$, and recompute the $\Omega_{h,l}$ and $p_{h,l}$ as before. Keep iterating until the process converges.

This procedure should also work for cold-star models with small surface densities much less than the average density, since the small surface-discontinuity should be negligible within our level of approximation.

ii) The Case for Which the Density ϵ is Strongly Discontinuous at the Stellar Surface

For this case the surface density is not negligible in comparison with the average density, and we have in mind especially the homogeneous models of § IV below. We have found that the method of the previous case requires three modifications if convergence is to be achieved.

First, the metric functions ν and ω have strongly discontinuous second radial derivatives at the stellar surface. This forces us to fit backward and forward Lagrangian polynomials to such functions on the inner and outer sides, respectively, of the stellar surface, in a way which explicitly guarantees that the fits are $C^{(1)}$ across the surface.

The method of spline fitting provides a technique for ensuring the appropriate amount of smoothness. Let \mathcal{H}_l be the value of h at the first grid point outside the stellar surface along the l th spoke. We write down the modified Lagrangian-polynomial fits

$$f(r, \mu_l) \approx f_{<}(r, \mu_l) = \sum_{i=\mathcal{H}_l-n}^{\mathcal{H}_l-1} f(i\Delta r, \mu_l) \prod_{j=\mathcal{H}_l-n, j \neq i}^{\mathcal{H}_l-1} \left(\frac{r-j\Delta r}{i\Delta r-j\Delta r} \right) + a_{<l} \prod_{i=\mathcal{H}_l-n}^{\mathcal{H}_l-1} (r-i\Delta r) \quad (59a)$$

near $r = (\mathcal{H}_l - 1)\Delta r$ inside the surface, and

$$f(r, \mu_l) \approx f_{>}(r, \mu_l) = \sum_{i=\mathcal{H}_l}^{\mathcal{H}_l+n-1} f(i\Delta r, \mu_l) \prod_{j=\mathcal{H}_l, j \neq i}^{\mathcal{H}_l+n-1} \left(\frac{r-j\Delta r}{i\Delta r-j\Delta r} \right) + a_{>l} \prod_{i=\mathcal{H}_l}^{\mathcal{H}_l+n-1} (r-i\Delta r) \quad (59b)$$

near $r = \mathcal{H}_l\Delta r$ outside the surface. Here n is the number of grid points (4 or 5, say) used to fit the polynomials. The constants $a_{<l}$ and $a_{>l}$ are determined by the conditions

$$f_{<}(r^*_l, \mu_l) = f_{>}(r^*_l, \mu_l), \quad (59c)$$

$$f_{<,r}(r^*_l, \mu_l) = f_{>,r}(r^*_l, \mu_l), \quad (59d)$$

where r^*_l is the position of the stellar surface along the l th ray. The value of r^*_l might be determined, for example, either by fitting a polynomial to the pressure and finding its zero or by assuming that $r^*_l = \mathcal{H}_l\Delta r$.

Differentiation of equations (59a) and (59b) yields backward formulae for radial derivatives at $r = (\mathcal{H}_l - 1)\Delta r$ and forward formulae at $r = \mathcal{H}_l\Delta r$. The usual formulae (46) and (47) are used at other values of r . Hence the difference equations of case (i) are modified at $h = \mathcal{H}_l - 1$ or \mathcal{H}_l in a way we shall not take the trouble to write down.

A second complication involves the matter terms proportional to $\partial p/\partial v$ or $\partial \epsilon/\partial v$ on the left-hand sides of equations (50a) and (50b). Particularly for constant- ϵ models, these terms are large even near the surface. The corrections $\delta v_{h,l}$ are consequently rather sensitive to these terms, and they tend to oscillate unstably unless corrective measures are taken.

We have found that the oscillations can be suppressed by the insertion of a multiplicative "convergence factor" of the form $c_1 + c_2(1 - r/r^*_l)$ in front of the terms proportional to $\partial p/\partial v$ or $\partial \epsilon/\partial v$ on the left-hand sides of equations (50a) and (50b). Proper adjustment of the constants c_1 and c_2 enables us to achieve convergence.

A third complication involves the elusiveness of convergence in the present case when the constant β (cf. § II d) is held fixed from one stage to the next. Fortunately, there is again a remedy: convergence can be achieved if, instead of β , the rest mass

$$M_0 = \int \mu_B n (1 - v^2)^{-1/2} B e^{2\zeta - 3\nu} 2\pi r^2 dr d\mu, \quad (60)$$

where μ_B is the rest mass per baryon, is held fixed. From a mathematical point of view, it is rather remarkable that this constraint, though physically reasonable, is required, since the rest mass does not appear anywhere in the basic structure equations.

A successful method for computing models with severe density discontinuities at the stellar surface is the following.

Fix, once and for all, the equations of state, the rotation law, Ω_A , and M_0 . Incorporate the first two modifications just discussed into the linearized equations of case (i). (We should remark that in our actual computations of the homogeneous bodies discussed below, 5-point difference formulae were used everywhere in order to maximize accuracy.) Then proceed just as in case (i), except for this: at each stage, demand that β be readjusted to keep the value of the rest mass fixed.

This completes our discussion of the basic numerical method.

IV. UNIFORMLY ROTATING HOMOGENEOUS BODIES

In this section we shall discuss the results we have obtained for uniformly rotating (constant Ω) homogeneous (constant ϵ) bodies. Bonazzola and Schneider (1974) previously studied these bodies, but there is only a small overlap between our more extensive results and theirs.

There are a number of reasons why one might want to study these relativistic analogues of the classical Newtonian Maclaurin spheroids (see Chandrasekhar 1969 for a comprehensive discussion of the Newtonian bodies), even though at first sight they might appear to be somewhat unrealistic. First, for many of the proposed cold equations of state, the more massive neutron-star models have nearly uniform distributions of density over central regions containing most of the mass. Second, Ostriker and his co-workers (see, e.g., Bodenheimer and Ostriker 1973) have demonstrated the existence of a remarkably close correspondence between many of the properties of the Maclaurin spheroids and those of more realistic, Newtonian fluid bodies. Third, the relativistic bodies afford the opportunity to explore the effect of rotation in situations involving extreme strengths of relativity: in the nonrotating limit,

homogeneous bodies have ratios $(2GM/c^2 r_s^*)$ of gravitational radius to Schwarzschild-coordinate radius that can be as large as 8/9.

a) *Some Details Involved in Constructing the Solutions*

The explicit equations for homogeneous bodies are those of incompressible matter,

$$\epsilon = \text{constant}, \quad \mu_B n = \epsilon, \quad (61)$$

and the rotation law for uniform rotation is

$$u^\phi/u^t = \Omega = \text{constant}. \quad (62)$$

The integral (23) of the equations of motion then becomes

$$\frac{p}{\epsilon} = \frac{1 - \gamma}{e^{\nu}(1 - v^2)^{1/2}} - 1, \quad (1 - \gamma) \equiv \beta^{1/2}. \quad (63)$$

The relaxed matter terms on the left-hand sides of the difference equations of § III can now be evaluated explicitly at each grid point by eliminating p via equation (63). Note that, for example,

$$\begin{aligned} \partial p/\partial \nu &= -(\epsilon + p)(1 + v^2)/(1 - v^2) && \text{inside star} \\ &= 0 && \text{outside star}. \end{aligned} \quad (64)$$

The assumption $\partial \epsilon/\partial \nu = 0$ at all grid points is implicit in this equation. This is all right because the computer always places the surface, where $\partial \epsilon/\partial \nu$ has a delta-function singularity, somewhere between two grid points.

We find it convenient to use ϵ as a scaling parameter by taking $\epsilon^{-1/2}$ to be a fundamental unit of length in our calculations. A quantity such as $M_0 \epsilon^{1/2}$ then measures the strength of relativity, and a quantity such as Bardeen's (1971) rotation parameter

$$R \equiv J^2 \epsilon^{1/3} / M_0^{10/3} \quad (65)$$

then measures the amount of rotation.

We build up sequences of rotating bodies by beginning with a spherical body. A spherical body is specified by its value

$$\gamma_s = 1 - (1 - 2M/r_s^*)^{1/2} \quad (66)$$

of γ in equation (63). Here r_s^* is the value of the Schwarzschild radial coordinate r_s at the surface of the body; and M is the mass, which satisfies

$$M = (4\pi/3)r_s^{*3}\epsilon. \quad (67)$$

The relation between r_s and our radial coordinate r is

$$\begin{aligned} r_s &= \frac{2r/c_3}{1 + (8\pi\epsilon r^2/3c_3^2)} && \text{inside star} \\ &= r(1 + \frac{1}{2}M/r)^2 && \text{outside star}, \end{aligned} \quad (68a)$$

where

$$c_3 \equiv \frac{1}{2}[1 - M/r_s^* + (1 - 2M/r_s^*)^{1/2}][1 + (1 - 2M/r_s^*)^{1/2}]. \quad (68b)$$

In the spherical limit, the metric functions are given by

$$\begin{aligned} e^\nu &= \frac{3}{2}(1 - 2M/r_s^*)^{1/2} - \frac{1}{2}[1 - (8\pi/3)\epsilon r_s^{*2}]^{1/2} && \text{inside star} \\ &= 1 - 2M/r_s && \text{outside star}, \end{aligned} \quad (69a)$$

$$e^\zeta = B = (r_s/r)e^\nu, \quad (69b)$$

and

$$\omega = 0. \quad (69c)$$

Having determined a spherical model in units of ϵ by specifying γ_s , we find its value of $M_0 \epsilon^{1/2}$ from equation (60). We then choose a small value, say ~ 0.1 , for $\Omega \epsilon^{1/2}$, and apply our iterative procedure. In doing so, we readjust β ,

or γ , at each stage by repetitive application of Newton's relation in the form

$$\Delta\gamma = \frac{(\text{desired value of } M_0) - (\text{present value of } M_0)}{\partial M_0 / \partial \gamma}, \quad (70a)$$

where

$$\frac{\partial M_0}{\partial \gamma} = -\frac{4\pi}{1-\gamma} \int_0^1 d\mu \left[v_{,r} - \frac{vv_{,r}}{1-v^2} \right]^{-1} \frac{\mu_B n}{(1-v^2)^{1/2}} B e^{2r-3v}, \quad (70b)$$

and $\Delta\gamma$ is the change in γ . After achieving convergence to a model with a given value of $\Omega\epsilon^{-1/2}$, we increase this quantity a little and try to construct a new model (there is no guarantee that one exists). In this way we build up a sequence of models with fixed $M_0\epsilon^{1/2}$ and with varying $\Omega\epsilon^{-1/2}$ and R .

b) Results

Our results for uniformly rotating homogeneous bodies are contained in Figures 1-7, Tables 1-4, and the text below. Various checks, involving comparisons with the fully relativistic slow-rotation calculations of Chandrasekhar

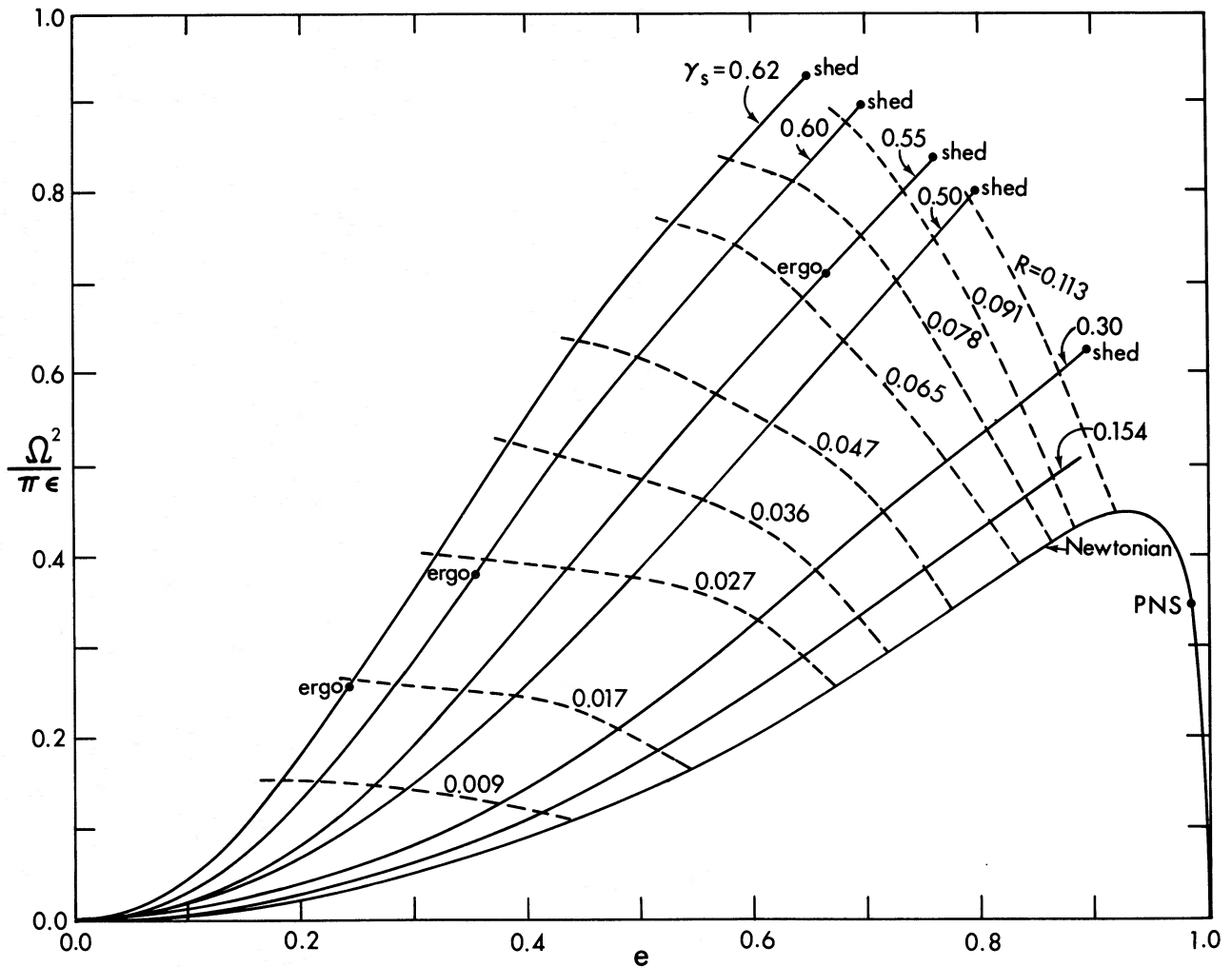


FIG. 1.—A plot of the square of the uniform angular velocity, in units π times ϵ , versus the eccentricity (eq. [71]) of homogeneous bodies. The bottom solid curve is the Newtonian Maclaurin sequence. The other solid curves are relativistic sequences of fixed (rest mass) $\times \epsilon^{1/2}$. Each is associated with a particular value of γ_s , defined by eq. (66). The dashed curves are curves of constant rotation parameter R (eq. [65]). At the Newtonian point marked PNS, the post-Newtonian corrections to the Maclaurin spheroids become singular. At the points marked SHED, centrifugal forces balance gravity at the equator, and the sequences terminate. At the points marked ERGO, there appear regions within which observers must rotate relative to the distant stars.

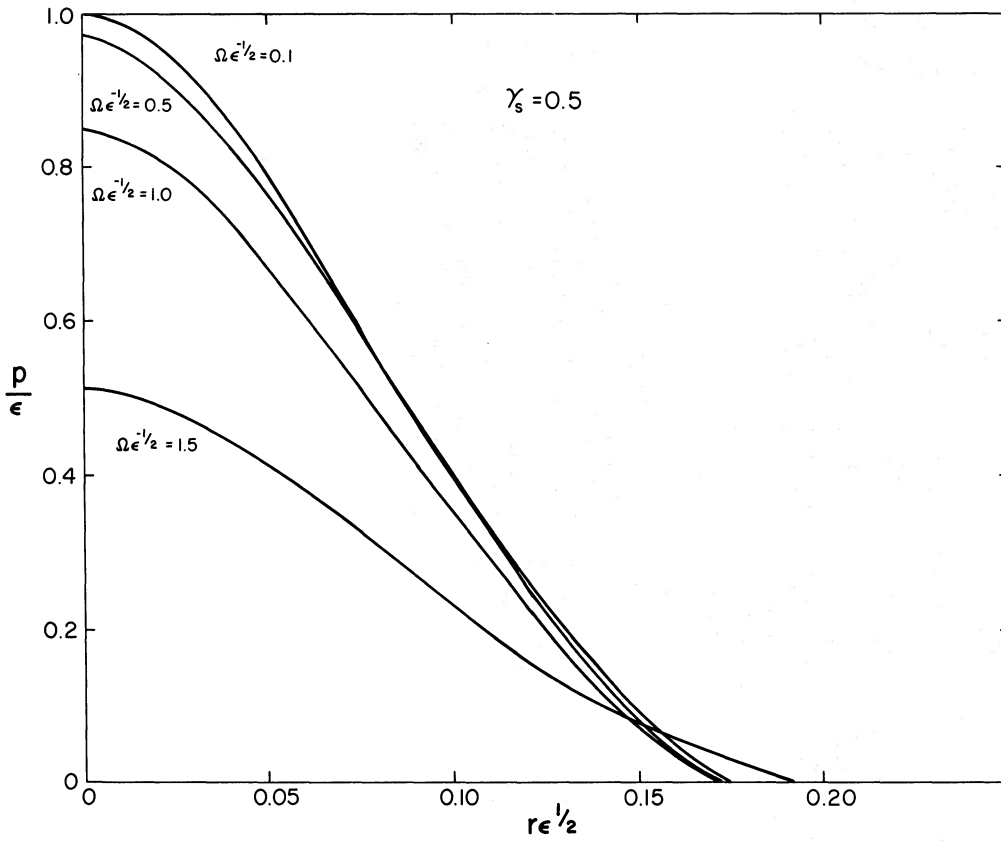


FIG. 2.—A plot of the equatorial pressure p , in units ϵ , versus the radial coordinate, in units $\epsilon^{-1/2}$, for various configurations along the sequence with $\gamma_s = 0.5$. Ω is the angular velocity of a configuration.

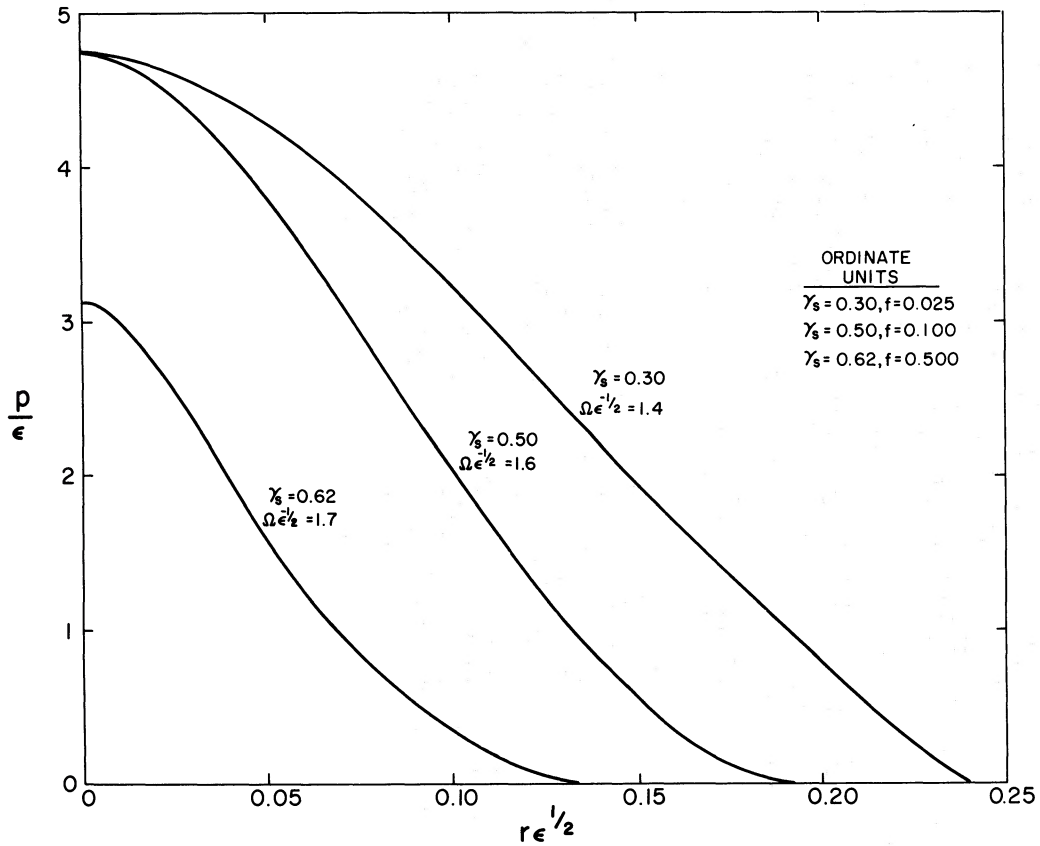


FIG. 3.—A plot of the equatorial pressure p , in units ϵ , versus the radial coordinate, in units $\epsilon^{-1/2}$, for configurations near the shed points along three relativistic sequences. Ω is the angular velocity of a configuration. The factor f is the amount by which exhibited values of p/ϵ must be multiplied to yield the correct values.

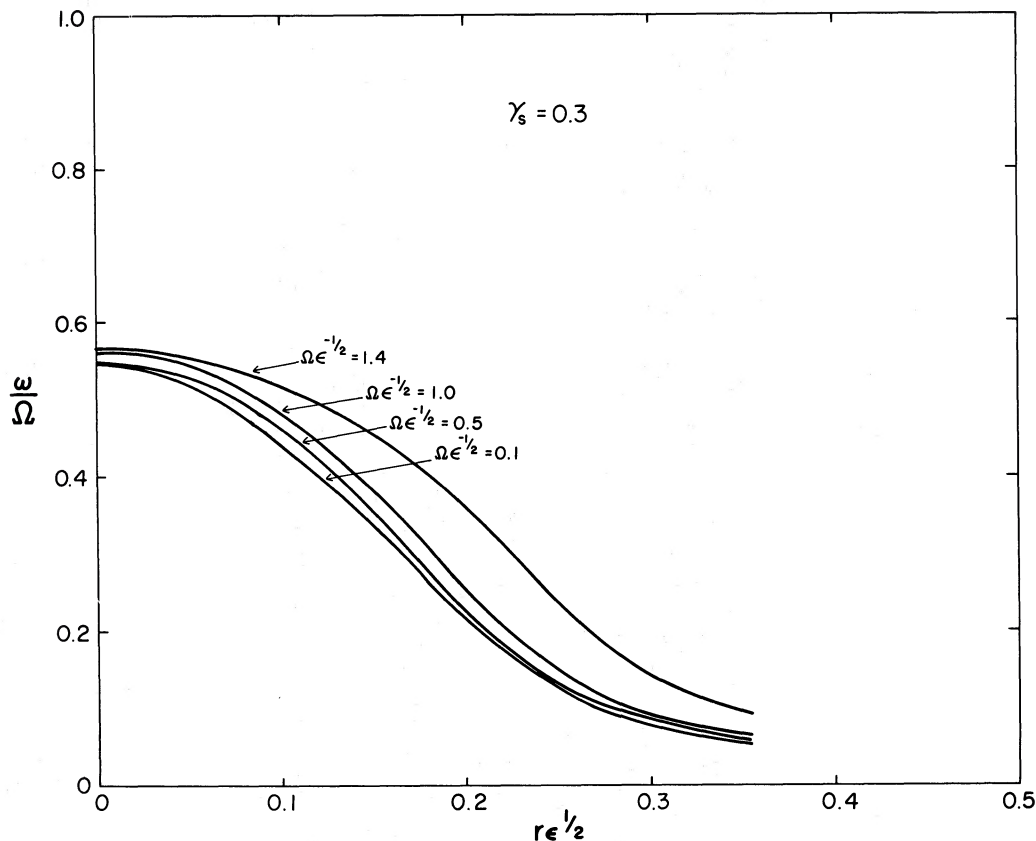


FIG. 4.—A plot of the percent of dragging, ω/Ω , versus the radial coordinate, in units $\epsilon^{-1/2}$, throughout the equatorial plane for various configurations along the sequence with $\gamma_s = 0.3$. Ω is the angular velocity of a configuration.

TABLE 1
THE SEQUENCE WITH $\gamma_s = 0.3$, $M_0\epsilon^{1/2} = 0.077^*$

e	$\Omega\epsilon^{-1/2}$	R	t_N	ω_c/Ω	v_e	$10^3 I\epsilon^{3/2}$	γ	p_c/ϵ	E_B/M_0
0.063	0.10	0.0002	0.0007	0.5365	0.027	2.03	0.300	0.272	0.178
0.12	0.20	0.0009	0.0030	0.5370	0.054	2.03	0.301	0.271	0.178
0.18	0.30	0.0020	0.0067	0.5378	0.082	2.05	0.302	0.269	0.177
0.24	0.40	0.0036	0.012	0.5391	0.11	2.06	0.303	0.266	0.176
0.30	0.50	0.0057	0.019	0.5406	0.14	2.08	0.305	0.263	0.175
0.36	0.60	0.0084	0.028	0.5426	0.16	2.11	0.308	0.258	0.173
0.42	0.70	0.012	0.039	0.5449	0.19	2.15	0.311	0.252	0.171
0.48	0.80	0.016	0.052	0.5476	0.22	2.20	0.314	0.245	0.169
0.54	0.90	0.022	0.067	0.5507	0.25	2.25	0.318	0.236	0.166
0.60	1.0	0.028	0.086	0.5542	0.28	2.33	0.323	0.226	0.162
0.66	1.1	0.038	0.11	0.5581	0.32	2.44	0.328	0.212	0.157
0.73	1.2	0.051	0.14	0.5620	0.36	2.60	0.333	0.194	0.150
0.80	1.3	0.075	0.19	0.5657	0.41	2.90	0.340	0.168	0.139
0.90	1.4	0.15	0.31	0.5667	0.46	3.81	0.351	0.118	0.108

* The quantity γ_s is defined by equation (66). All members of the sequence have the same value of $M_0\epsilon^{1/2}$, where M_0 is the rest mass and ϵ is the density of mass energy. The various columns are the following: e , the eccentricity (eq. [71a]); $\Omega\epsilon^{-1/2}$, the angular velocity of the fluid relative to infinity, in the unit $\epsilon^{1/2}$; R , the rotation parameter $J^2\epsilon^{1/3}/M_0^{10/3}$, where J is the angular momentum; t_N , the quantity $\frac{1}{2}J\Omega/(M_0 + \frac{1}{2}J\Omega - M)$, where M is the mass; ω_c/Ω , the angular velocity relative to infinity of the zero-angular-momentum observer (cf. § IIa) at the center of the body in the unit Ω ; v_e , the velocity (eq. [6]) of the fluid relative to the zero-angular-momentum observer at the equator; I , the moment of inertia J/Ω , in the unit $\epsilon^{-3/2}$; γ , the value of the constant appearing in the equation of equilibrium (63); p_c/ϵ , the pressure at the center of the body, in the unit ϵ ; E_B/M_0 , the fractional binding energy $1 - M/M_0$.

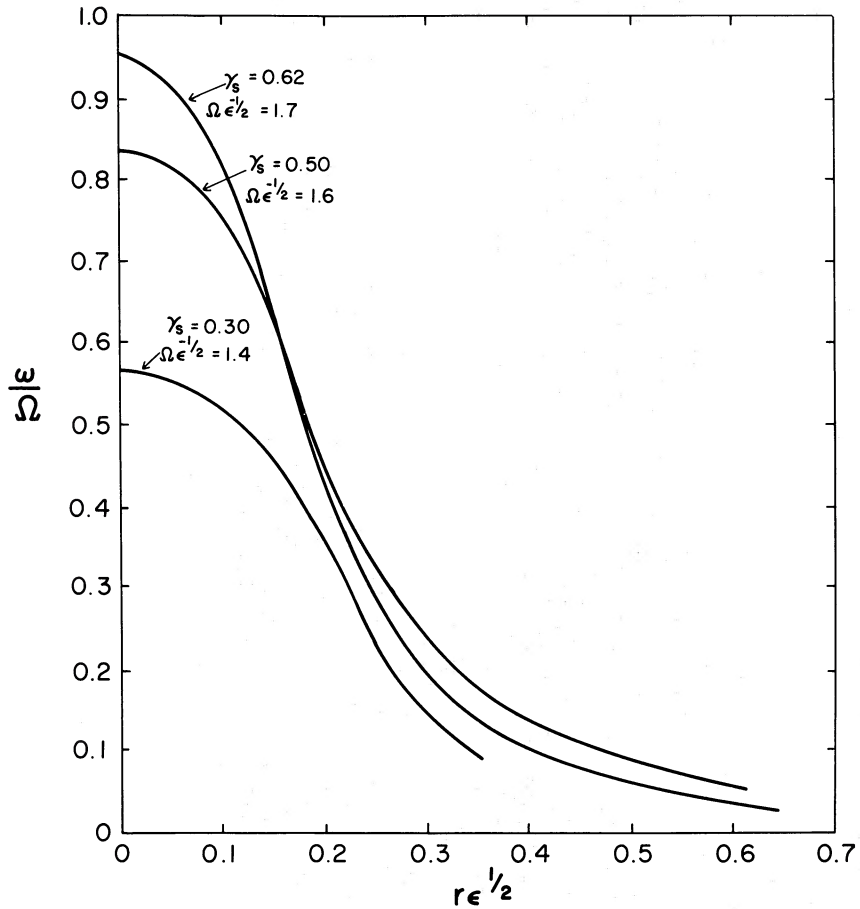


FIG. 5.—A plot of the percent of dragging, ω/Ω , versus the radial coordinate, in units $\epsilon^{-1/2}$, throughout the equatorial plane for configurations near the shed points along three relativistic sequences. Ω is the angular velocity of a configuration.

TABLE 2
THE SEQUENCE WITH $\gamma_s = 0.5, M_0\epsilon^{1/2} = 0.16^*$

e	$\Omega\epsilon^{-1/2}$	R	t_N	ω_c/Ω	v_e	$10^3 I\epsilon^{3/2}$	γ	p_c/ϵ	E_B/M_0
0.045	0.1	0.0002	0.0007	0.8214	0.032	6.58	0.500	0.999	0.294
0.085	0.2	0.0008	0.0028	0.8215	0.064	6.59	0.501	0.994	0.294
0.13	0.3	0.0018	0.0063	0.8218	0.096	6.61	0.503	0.985	0.293
0.17	0.4	0.0032	0.011	0.8222	0.13	6.64	0.505	0.975	0.291
0.22	0.5	0.0051	0.018	0.8228	0.16	6.69	0.508	0.962	0.289
0.26	0.6	0.0075	0.026	0.8236	0.20	6.74	0.511	0.945	0.287
0.31	0.7	0.010	0.036	0.8245	0.23	6.81	0.516	0.924	0.284
0.35	0.8	0.014	0.047	0.8255	0.26	6.89	0.521	0.899	0.280
0.40	0.9	0.018	0.060	0.8266	0.30	6.98	0.526	0.870	0.276
0.45	1.0	0.023	0.076	0.8276	0.33	7.12	0.533	0.836	0.271
0.50	1.1	0.029	0.094	0.8286	0.36	7.27	0.540	0.795	0.265
0.55	1.2	0.037	0.12	0.8295	0.40	7.47	0.548	0.746	0.258
0.61	1.3	0.046	0.14	0.8302	0.43	7.74	0.557	0.687	0.249
0.67	1.4	0.060	0.18	0.8305	0.47	8.17	0.567	0.613	0.237
0.75	1.5	0.084	0.23	0.8297	0.55	9.05	0.579	0.513	0.217
0.79	1.6	0.11	0.30	0.8313	0.61	9.82	0.596	0.472	0.187

* The notation is the same as in Table 1.

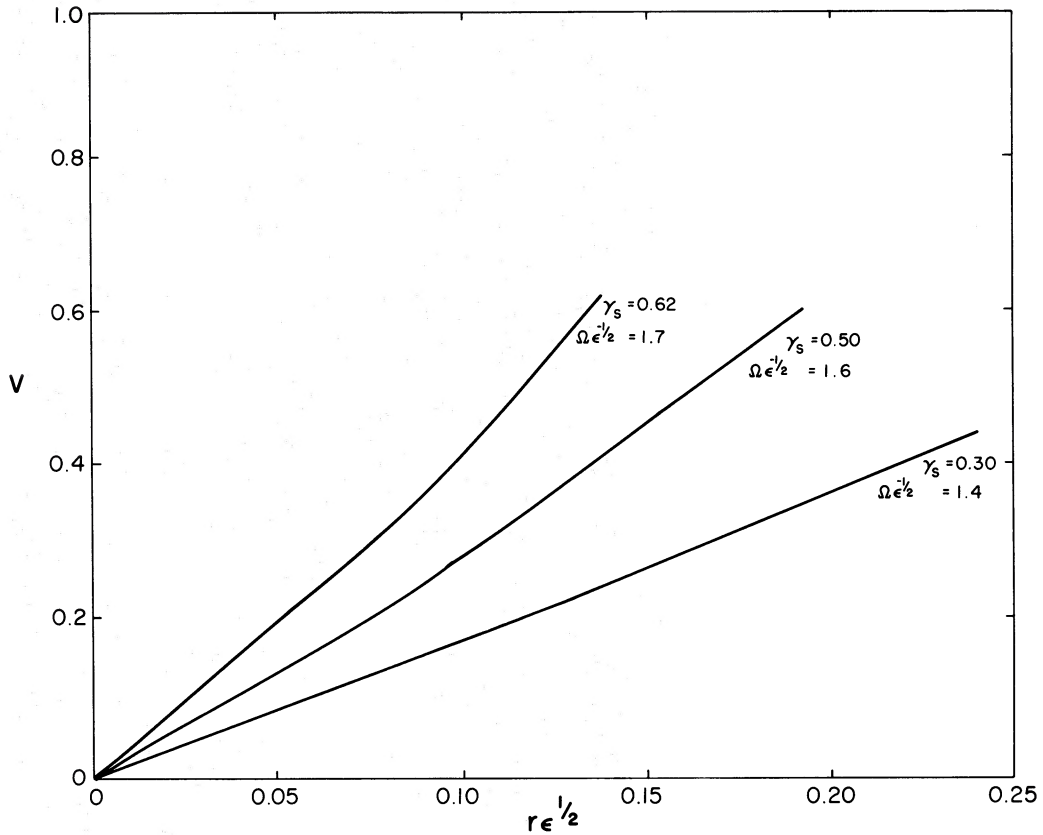


FIG. 6.—A plot of the velocity v of the fluid relative to the local zero-angular-momentum observer (eq. [6]) versus the coordinate radius, in units $\epsilon^{-1/2}$, throughout the equatorial plane for configurations near the shed points along three relativistic sequences. Ω is the angular velocity of a configuration.

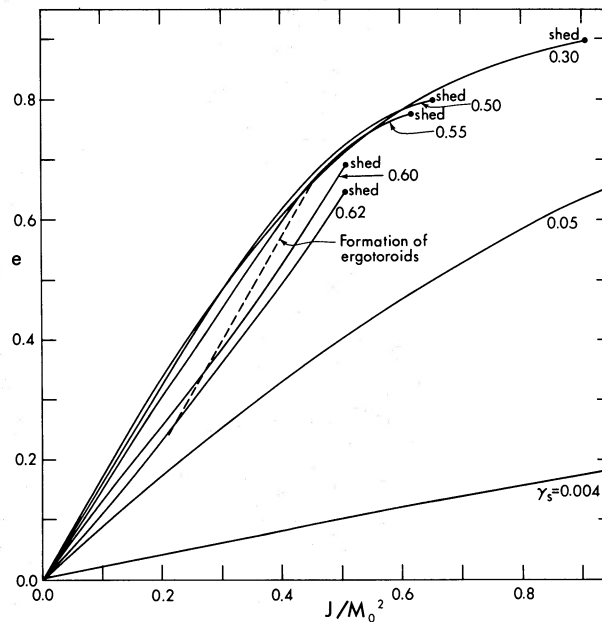


FIG. 7.—A plot of eccentricity (eq. [71]) versus the ratio J/M_0^2 , where J is the angular momentum and M_0 is the rest mass, for various relativistic sequences. The dashed curve marks the appearance of regions within which observers must rotate relative to the distant stars. At the points marked SHED, centrifugal forces balance gravity at the equator, and the sequences terminate.

TABLE 3
THE SEQUENCE WITH $\gamma_s = 0.62$, $M_0\epsilon^{1/2} = 0.215^*$

e	$\Omega\epsilon^{-1/2}$	R	t_N	ω_e/Ω	v_e	$10^2 J\epsilon^{3/2}$	γ	p_e/ϵ	E_B/M_0
0.032	0.1	0.0002	0.0007	0.9594	0.031	1.06	0.620	4.45	0.363
0.078	0.3	0.0017	0.0061	0.9595	0.094	1.06	0.623	4.37	0.361
0.106	0.4	0.0030	0.011	0.9595	0.12	1.06	0.625	4.31	0.359
0.157	0.6	0.0069	0.025	0.9595	0.19	1.07	0.633	4.15	0.353
0.186	0.7	0.0095	0.034	0.9593	0.22	1.08	0.638	4.04	0.350
0.214	0.8	0.013	0.045	0.9593	0.25	1.08	0.644	3.91	0.346
0.245	0.9	0.016	0.057	0.9591	0.29	1.09	0.651	3.77	0.341
0.276	1.0	0.021	0.071	0.9584	0.31	1.11	0.659	3.60	0.337
0.312	1.1	0.026	0.088	0.9578	0.35	1.13	0.667	3.41	0.330
0.350	1.2	0.032	0.11	0.9571	0.39	1.14	0.676	3.18	0.323
0.392	1.3	0.039	0.13	0.9562	0.44	1.17	0.686	2.92	0.314
0.440	1.4	0.047	0.15	0.9550	0.46	1.19	0.698	2.64	0.304
0.495	1.5	0.057	0.18	0.9534	0.51	1.23	0.710	2.32	0.292
0.572	1.6	0.075	0.23	0.9507	0.57	1.32	0.724	1.99	0.267
0.643	1.7	0.094	0.27	0.9487	0.63	1.39	0.741	1.58	0.250

* The notation is the same as in Table 1.

and Miller (1974) and the post-Newtonian calculations of Bardeen (1971), involving the Hartle-Sharp (1967) variational principle for rotating relativistic stars in a manner explained below, and involving tests on how changes in grid structure influence results, indicate that our results are accurate to a couple of percent.

i) *A Comparison of the Newtonian and Relativistic Sequences*

Some of the differences between the Newtonian and the relativistic bodies are evident in Figure 1, which is a plot of the square of the angular velocity (in the unit $\pi\epsilon$) of a model versus its eccentricity

$$e \equiv [1 - (d_p/d_e)^2]^{1/2}; \quad (71)$$

here the quantities

$$d_p \equiv \int_0^{r^*(\mu=1)} dr e^{\zeta-\nu}, \quad d_e \equiv \int_0^{r^*(\mu=0)} dr e^{\zeta-\nu} \quad (72)$$

are the proper radial distances from the center of a body to its surface along the rotation axis and in the equatorial plane, respectively, within a 3-surface orthogonal to the zero-angular-momentum observers. The bottom solid curve is the Newtonian Maclaurin sequence. All Newtonian models can be represented by this single sequence, since in Newtonian theory there is another scaling parameter, say the Newtonian mass M_0 , in addition to ϵ . (A third parameter, say e or R , then measures the amount of rotation.) The solid curves above the Newtonian curve are relativistic sequences along which $M_0\epsilon^{1/2}$ is constant. Each sequence is labeled by the value of $\gamma = \gamma_s$ for the spherical member of the sequence. Sequences with larger values of γ_s (and $M_0\epsilon^{1/2}$) are more relativistic. The dashed curves are of constant values of R in equation (65); and they show the relative locations of relativistic and Newtonian models with the same ϵ , M_0 , and J : for given values of $J\epsilon$ and $M_0\epsilon^{1/2}$, there is one relativistic point and one Newtonian point, both lying on the same dashed curve of constant R .

Figure 1 and also Tables 1–3 show that larger strengths of relativity require larger angular velocities to produce a given value of e or of R . This reflects the importance for these bodies of the dragging of inertial frames and the fact that, roughly speaking, the centrifugal forces are proportional to v^2 and the angular-momentum density is proportional to v , while $v \propto (\Omega - \omega)$ (cf. eq. [6]), and ω/Ω increases with γ_s at fixed e or R . Note that e and R do not measure rotation in the same way and that e decreases as γ_s increases at fixed R . This appears to be because the

TABLE 4
THE POINTS OF FORMATION OF ERGOTOROIDS ALONG SEQUENCES*

γ_s	γ	e	$\Omega\epsilon^{-1/2}$	R	t_N	J/M^2
0.55	0.63	0.67	1.5	0.07	0.20	0.83
0.60	0.64	0.36	1.1	0.026	0.089	0.59
0.62	0.65	0.24	0.9	0.016	0.057	0.49

* The quantities in the first six columns are defined in the same way as in Table 1. The quantity J/M^2 is the ratio of the angular momentum to the square of the mass-energy.

proper volume gets very big in the central regions of highly relativistic models; the major contributions to proper radii then come from these nearly spherical central regions where rotational effects are small; and the differences between proper radii in different directions thus tend to decrease as γ_s increases at fixed R .

Along the Newtonian sequence, Ω first increases with e , reaches a maximum given by $\Omega_{\max}^2 \approx 0.449\pi\epsilon$ at $e \approx 0.93$, and thereafter decreases toward zero as $e \rightarrow 1$. For e close to unity, $\Omega^2 \propto d_e^{-3}$ in accord with the Keplerian behavior of the outermost fluid orbits. In Newtonian theory the centrifugal force is proportional to r and the gravitational force is nearly so in the outer regions of highly flattened, constant- ϵ , constant- Ω fluids. This delicate balance permits Maclaurin spheroids at all possible values of e .

The balance is destroyed by relativistic effects. Our calculations show that at least for $\gamma_s \gtrsim 0.3$, and very probably for all γ_s , the relativistic sequences terminate at points marked "shed" in Figure 1. At these points centrifugal forces balance gravity at the equator. Numerical instabilities have prevented us from verifying that sequences with small values of γ_s terminate, but we have little doubt that they do. The line through the shed points in Figure 1 probably extends down to the point marked PNS, where the post-Newtonian corrections to the Maclaurin spheroids become singular (Chandrasekhar 1967; Bardeen 1971). Such a behavior agrees with Bardeen's (1971) prediction that uniformly rotating, homogeneous, relativistic models become untenable at values of R which decrease from the PNS value ~ 0.273 as γ_s increases from zero. The value of R at the termination, or shed, points drops to ~ 0.095 for the sequence with $\gamma_s = 0.62$. Bardeen (1971) has shown that the PNS point is also the point at which the Maclaurin spheroids become secularly unstable to axisymmetric differential rotation. It may be that the relativistic bodies also become secularly unstable to differential rotation before the sequences terminate. In any event, the sequences terminate due to shedding of matter, because of the artificial constraint of uniform rotation; and differentially rotating homogeneous bodies are expected to exist at values of R larger than those at the shed points.

ii) The Formation of Ergotoroids

A fundamentally relativistic phenomenon is associated with the points marked ERGO on the sequences with $\gamma_s \geq 0.55$ in Figure 1. In every model above the ergopoint on a sequence, there is a topologically toroidal region, called an ergoregion or ergotoroid, in which the dragging of inertial frames is so strong that all observers are forced to rotate with angular velocity $d\phi/dt > 0$ relative to the distant stars. Mathematically, an ergoregion is the collection of points at which the metric component $g_{tt} > 0$, and hence at which the Killing vector ξ^a that is timelike at infinity is spacelike. For our models the ergoregions cannot contain any part of the rotation axis, and hence must be toroidal, for the following reason: we have assumed that the fluid 4-velocity u^a is a linear combination of the Killing vectors ξ^a and η^a (cf. § IIa); but $\eta^a = 0$ on the rotation axis; hence $u^a \propto \xi^a$ on the rotation axis, and ξ^a cannot be spacelike there.

Table 4 exhibits the approximate values of various parameters associated with the ergopoints on three sequences. It is clear that the ergopoints appear at smaller amounts of rotation as the strength of relativity increases: the values of the eccentricity e , the rotation parameter R , and the quantity

$$t_N \equiv \frac{1}{2}J\Omega / (M_0 + \frac{1}{2}J\Omega - M), \quad (73)$$

which reduces to the ratio of rotational kinetic energy to gravitational potential energy in the Newtonian limit, all decrease at the ergopoints as γ_s increases.

Along the sequence of infinitesimally thin, uniformly rotating, pressureless disks of Bardeen and Wagoner (1971), ergotoroids first appear at the rim of a disk. Along one of our sequences, however, the ergotoroids first appear at a point in the equatorial plane between the center and the surface of a model. (Wilson 1972 also found this behavior.) As shown in Figure 2 of Butterworth and Ipser (1975) for the sequence with $\gamma_s = 0.61$, the ergotoroids grow with increasing rotation and can eventually reach into the exterior vacuum.

iii) The Radial Behavior of Various Quantities

Figure 2 shows how the pressure distribution in the equatorial plane steepens as a stellar model of fixed rest mass and fixed equation of state (fixed density in the present case) spins down along the sequence with $M_0\epsilon^{1/2} = 0.16$, $\gamma_s = 0.5$. This behavior results in the expected decrease in the moment of inertia,

$$I \equiv J/\Omega, \quad (74)$$

as shown in Table 2.

Figure 3 compares the pressure distributions in the equatorial planes of configurations near the termination points along three different relativistic sequences. The pressure distribution steepens and the equatorial coordinate radius, in the unit $\epsilon^{-1/2}$, decreases as the strength of relativity increases. But $M_0\epsilon^{1/2}$ and $M\epsilon^{1/2}$ increase sufficiently rapidly to cause the moment of inertia, in the unit $\epsilon^{-3/2}$, to increase.

Figure 4 shows the percent of dragging, ω/Ω , throughout the equatorial planes of various configurations along the sequence with $\gamma_s = 0.3$. As a model of fixed rest mass M_0 and fixed density ϵ spins down along the sequence, ω/Ω decreases at a given coordinate radius. This behavior is not common to all sequences, however. For example, as Table 3 reveals, the percent of dragging at $r = 0$ can decrease with $J\epsilon$ over parts of highly relativistic sequences. In any case, the behavior of ω/Ω can never cause the moment of inertia to increase as $J\epsilon$ decreases.

Figure 5 shows ω/Ω throughout the equatorial planes of configurations near the termination points along different sequences, and Figure 6 shows the corresponding velocity v of the fluid relative to the zero-angular-momentum observers. At a fixed fraction of the equatorial radius of a model, ω/Ω increases with the strength of relativity. The velocity v varies almost linearly with the radial coordinate r ; but in highly relativistic configurations it is much larger than the Newtonian value Ωr , due to the factor $e^{-2\nu}$ in the definition of v arising from time dilation and the increase in the ratio of proper distance to coordinate distance in strong gravitational fields.

iv) Stability

We have not yet performed any stability calculations for our models, so the following discussion is somewhat speculative.

We previously mentioned one type of instability to which our models might succumb, the axisymmetric secular instability to differential rotation that would be excited by any operative viscosity. If a body reached a point of onset of this instability, it would begin to rotate differentially. The body might then form a configuration with a nearly uniformly rotating central bulge that continually transfers its angular momentum to a surrounding differentially rotating disk.

Other types of instabilities, however, that grow on shorter time scales probably appear before the above secular instability and play the dominant roles.

One of these is a nonaxisymmetric dynamical instability, the so-called Dedekind bar-mode instability, which is excited by gravitational radiation-reaction in general relativity, and which is present in nearly Newtonian models with $e \geq 0.813$, $R \geq 0.0572$ (Chandrasekhar 1970; Friedman and Schutz 1975). This instability has spherical-harmonic index $|m| = 2$, and the corresponding mode radiates away angular momentum as well as energy. We expect that this instability sets in at certain values of $R \leq 0.0572$ for $\gamma_s > 0$.

Another dynamical instability is deeply relativistic. Ever since Penrose (1969) devised his classic process for extracting energy from ergoregions, it has been suspected that, as long as black-hole event horizons are absent, reasonable systems with ergoregions are dynamically unstable. Friedman (1975) has recently provided a proof that this is so for all fluid stellar models. Roughly speaking, stellar models with ergoregions are unstable for the following reason. The Killing vector ξ^a that is timelike at infinity tips over and becomes spacelike within an ergoregion. Hence one can set up there a non-axisymmetric perturbation that in some sense has negative energy relative to infinity. As the perturbation leaks out of the ergoregion and radiates energy, which must be positive, away to infinity, its amplitude within the ergoregion must actually grow and make the energy even more negative there in order to conserve total energy. The result is that the perturbation grows exponentially in time, and the system is unstable.

If, as we expect, the Dedekind instability sets in at $R \leq 0.0572$, for relativistic models, then Figure 1 shows that it sets in along a sequence before the ergoregion instability does when $\gamma_s \leq 0.57$ and perhaps later when $\gamma_s \geq 0.57$. Theoretically, incompressible models are always stable against overall collapse, so one could argue that the ergoregion instability is dominant for sequences with $\gamma_s \geq 0.57$. Actually, though, it is perhaps unlikely that there are any realistic stellar models corresponding to $\gamma_s \geq 0.57$ and stable to overall collapse. Thus we tend to be pessimistic about the existence of realistic stellar models that are completely stable up to the point of formation of ergotroids.

v) A Scenario for the Possible Evolution of Contracting Homogeneous Bodies

Figure 7 is a plot of eccentricity versus the ratio J/M_0^2 , and it provides a framework for discussing the slow contraction of bodies toward states of tighter binding. Our use of uniformly rotating bodies throughout this discussion may not be all that bad at first, since in Newtonian theory an initially uniformly rotating homogeneous body remains uniformly rotating if each mass element conserves its angular momentum during contraction.

Suppose that, due to axisymmetric emission of radiation, say, a body contracts at fixed angular momentum and rest mass. An initially weakly relativistic body evolving slowly in this way would first move vertically upward in Figure 7 in the direction of increasing γ_s as its density ϵ and its binding energy increase. If $J/M_0^2 \geq 0.5$, Figure 7 and the previous subsection indicate that the body eventually reaches a point of onset of the Dedekind instability. Our picture is that the instability timescale is less than the contraction timescale, and that the body is channeled to the left and down in Figure 7 in the direction of increasing γ_s along the line (not shown) of onset of the instability. The body next reaches either a point at which it undergoes overall gravitational collapse or a point on the dashed ergoregion-instability curve. In the former case, reasonable estimates for parameters at the collapse point might be $R \leq 0.057$, $\gamma_s \geq 0.4$. This corresponds to $J/M^2 \leq 0.8$ (at fixed R , J/M^2 is insensitive to γ_s) so that the body could collapse directly to a black hole without first having to get rid of more angular momentum. This means that it could bypass collapse to a disk. In the latter case, the ergoregion instability might drive the body down the dashed curve toward nearly spherical configurations, until overall collapse sets in. We remark that if the ergoregion instability is ever operative in realistic situations, it might lead to the emission of significant amounts of relatively high-frequency gravitational radiation. This is because, as Friedman (1975) has shown, the time scales associated with the ergoregion instability are inversely proportional to the spherical-harmonic index $|m|$ of a perturbation.

Consider now evolution when $J/M_0^2 \leq 0.5$ initially. A body proceeds vertically upward in Figure 7, reaches a maximum eccentricity $e \leq 0.7$ at $\gamma_s \sim 0.3$, and then proceeds downward in the direction of decreasing e until it collapses to a black hole. Even though e is decreasing, it is not completely clear that the body is contracting toward

states that are "more spherical." The problem is that, near the upper part of the range $0 \leq J/M_0^2 \leq 0.5$, rather than decreasing with e at fixed J/M_0^2 , R actually increases somewhat. It would be interesting to see whether the intrinsic deformation of the stellar surface, defined in some invariant way, behaves similarly.

The above scenario suggests that relativistic bodies might tend to avoid contracting to disklike configurations; and also that black holes might not generally be close to the Kerr limit $J = M^2$ at their formation. Of course, this could be all wrong if the required amounts of angular momentum cannot be radiated away during contraction and collapse.

vi) *Applications to Uniformly Rotating Neutron Stars*

We shall now use our results to obtain rough estimates of the amounts by which uniform rotation can increase the masses and moments of inertia of neutron stars. We remark first that the observed behavior of the pulsars, including that associated with the so-called glitches, does indicate that the neutron stars (thought to be) in pulsars are essentially uniformly rotating objects. Second, for many equations of state, the higher-mass neutron stars have nearly constant-density central regions that contain most of the matter, and our results are most appropriately applied to such objects.

We focus initially on the amount of rotational energy that can be stored in, and thereafter radiated away during spin-down of, a neutron star of fixed rest mass and fixed equation of state (approximated here as fixed density). In our approximation, if we forget about restrictions imposed by stability considerations, this energy is the difference between the mass-energy of the most rapidly rotating configuration (i.e., the one at the shed point) and that of the nonrotating configuration on a sequence of given $M_0\epsilon^{1/2}$ and γ_s . Suppose we assume $\epsilon \sim 5 \times 10^{15} \text{ g cm}^{-3}$ at the center of the nonrotating maximum-mass neutron star associated with a reasonable equation of state. Then the sequence with $\gamma_s = 0.3$ corresponds to neutron stars made of relatively soft matter, as is reflected by a relatively low value $M \sim 0.7 M_\odot$ for the nonrotating maximum mass; and the sequence with $\gamma_s = 0.5$ corresponds to neutron stars made of stiffer matter, as is reflected by a larger value $M \sim 1.3 M_\odot$ for the nonrotating maximum mass. Denoting by α the ratio of M for the most rapidly rotating configuration to M for the nonrotating configuration with the same M_0 and ϵ , we find from Tables 1 and 2 that $\alpha \sim 1.08$ for $\gamma_s = 0.3$ and $\alpha \sim 1.15$ for $\gamma_s = 0.5$. Smaller values of α are implied if the most rapidly rotating object is replaced by the last completely stable one along the sequence. In this case, assuming that the Dedekind instability sets in at $R \sim 0.057$, we obtain the smaller values $\alpha \sim 1.03$ for $\gamma_s = 0.3$ and $\alpha \sim 1.08$ for $\gamma_s = 0.5$. Thus the amount of rotational energy that can be stored should be $\geq 0.1 M_\odot$ if neutron-star matter is sufficiently stiff to yield a value $\geq 1.3 M_\odot$ for the maximum mass of a nonrotating neutron star.

The accuracy of our results for the change in mass-energy along a sequence of fixed $M_0\epsilon^{1/2}$ and γ_s can be checked by using the Hartle-Sharp (1967) variational principle for uniformly rotating relativistic stars. This principle implies that along one of our sequences of fixed M_0 , ϵ , and γ_s , changes in mass-energy are related to changes in angular momentum by the equation

$$\Delta M = \Omega \Delta J. \quad (75)$$

Our results in columns (2), (7), and (10) of Tables 1–3 agree with equation (74) to within a couple of percent.

During motion along a sequence of fixed γ_s , the moment of inertia, another important observable property of the neutron stars in pulsars, changes with the mass energy. For $\epsilon \sim 5 \times 10^{15} \text{ g cm}^{-3}$, our results in Tables 1 and 2 say the following: along the sequence with $\gamma_s = 0.3$, I varies from $\sim 1.2 \times 10^{44}$, in cgs units g cm^2 , for the nonrotating configuration to $\sim 1.5 \times 10^{44}$ for the configuration with $R = 0.057$ to $\sim 2.2 \times 10^{44}$ for the configuration at the shed point; along the sequence with $\gamma_s = 0.5$, the corresponding values for I are $\sim 3.8 \times 10^{44}$, 4.6×10^{44} , and 5.6×10^{44} .

Our results also provide us with a rough upper limit on the amount by which uniform rotation can increase the maximum possible mass of a neutron star above its nonrotating value, for a given equation of state. As the rotation increases, more matter can be supported in equilibrium, so the maximum rest mass M_0 , as well as M , increases above its nonrotating maximum value. It seems reasonable to assume that the ratio p/ϵ is nearly the same at the centers of the maximum-mass, nonrotating star and of the maximum-mass, uniformly rotating star obeying the same equation of state. Suppose we adopt this assumption and consider the example in which the maximum-mass, nonrotating configuration has central density $\sim 5 \times 10^{15} \text{ g cm}^{-3}$ and mass $M \sim 1.3 M_\odot$. This configuration is approximated by the nonrotating member of the sequence with $\gamma_s = 0.5$, which has a central ratio $p/\epsilon = 1$. If we first forget about restrictions imposed by stability considerations, the corresponding uniformly rotating configuration with the maximum possible mass should be the one that obeys the same equation of state (same ϵ here), has the same central ratio p/ϵ , and is rotating at the mass-shedding limit. Our results indicate that this latter configuration lies on a sequence with $\gamma_s \sim 0.6$ and has mass $M \sim 1.75 M_\odot$. Hence in this case uniform rotation increases the maximum mass of a neutron star by ~ 30 percent. A smaller percent increase is implied if we restrict attention to configurations that are completely stable. In this second case, the corresponding maximum-mass, rotating configuration has the same ϵ and p as before, but has a value of R that we take to be ~ 0.057 . This configuration lies on a sequence with $\gamma_s \sim 0.55$ and has mass $M \sim 1.5 M_\odot$. Hence in this second case uniform rotation increases the maximum mass by ~ 15 percent.

Finally, we note that for these cases the moment of inertia I increases from $\sim 3.8 \times 10^{44}$ g cm² for the nonrotating configuration to $\sim 5.3 \times 10^{44}$ g cm² for the last stable rotating configuration to $\sim 2.7 \times 10^{45}$ g cm² for the configuration at the shed point.

We thank J. M. Bardeen, S. Chandrasekhar, and J. L. Friedman for helpful discussions.

REFERENCES

- Bardeen, J. M. 1970, *Ap. J.*, **162**, 71.
 ———. 1971, *ibid.*, **167**, 425.
 Bardeen, J. M., and Wagoner, R. V. 1971, *Ap. J.*, **167**, 359.
 Bodenheimer, P., and Ostriker, J. P. 1973, *Ap. J.*, **180**, 159.
 Bonazzola, S., and Schneider, J. 1974, *Ap. J.*, **191**, 273.
 Butterworth, E. M., and Ipser, J. R. 1975, *Ap. J. (Letters)*, **200**, L103.
 Carter, B. 1973, in *Black Holes*, ed. C. De Witt and B. De Witt (New York: Gordon & Breach).
 Chandrasekhar, S. 1967, *Ap. J.*, **147**, 334.
 ———. 1969, *Ellipsoidal Figures of Equilibrium* (New Haven: Yale University Press).
 ———. 1970, *Ap. J.*, **161**, 561.
 Chandrasekhar, S., and Miller, J. C. 1974, *M.N.R.A.S.*, **167**, 63.
 Friedman, J. L. 1975, in preparation.
 Friedman, J., and Schutz, B. 1975, *Ap. J.*, **200**, 204.
 Hartle, J. B., and Sharp, D. H. 1967, *Ap. J.*, **147**, 317.
 Kerr, R. P. 1963, *Phys. Rev. Letters*, **11**, 522.
 Kopal, Z. 1961, *Numerical Analysis* (2d ed.; London: Chapman & Hall).
 Morse, P. M., and Feshbach, H. 1953, *Methods of Theoretical Physics* (New York: McGraw-Hill).
 Penrose, R. 1969, *Rev. Nuovo Cimento*, **1**, 252.
 Stoekly, R. 1965, *Ap. J.*, **142**, 208.
 Wilson, J. R. 1972, *Ap. J.*, **176**, 195.
 ———. 1973, *Phys. Rev. Letters*, **30**, 1082.

E. MANNING BUTTERWORTH and JAMES R. IPSER: Laboratory for Astrophysics and Space Research, University of Chicago, 933 E. 56th Street, Chicago, IL 60637